

11. LATE JURASSIC CARBONATE PLATFORM OF THE GALICIA MARGIN¹

L. F. Jansa, Atlantic Geoscience Centre, Geological Survey of Canada, Bedford Institute of Oceanography, Dartmouth, Nova Scotia, Canada

M. C. Comas, Instituto Andaluz de Geología Mediterránea, C.S.I.C., Universidad de Granada, Campus Universitario de Fuentenueva, Granada, Spain

M. Sarti, Dipartimento di Scienze della Terra, Università della Calabria, Cosenza, Italy
and

J. A. Haggerty, Department of Geosciences, The University of Tulsa, Tulsa, Oklahoma

ABSTRACT

The carbonate platform of Tithonian-?Berriasian age encountered on the western flank of the Galicia Bank at Site 639 is part of an extensive Late Jurassic carbonate shelf extending from Algarve to the Lusitanian Basin, Galicia Bank, and eastern Grand Banks of Newfoundland. The platform, which locally could be up to 400 m thick, probably overlies older sedimentary or low-grade metamorphic strata at Site 639. The 287 m of carbonates penetrated at this site was deposited mainly in shelf lagoon and shelf edge shoals, with localized low-relief biohermal mounds, in response to eustatic sea-level fluctuations and regional subsidence during the Tithonian-Berriasian. Minor block faulting influenced lithofacies distribution at the shelf edge. Shallow burial cementation was the most significant diagenetic event. After burial by several hundred meters of younger sediments, the top of the carbonate platform underwent extensive dolomitization during a period of tectonic fragmentation, followed by subaerial exposure and erosion of the platform. Such processes resulted in a complex carbonate diagenetic history with several periods of dolomitization. The major dolomitization event is the result of the replacement or mixing of formation fluids with evaporitic brines in a shallow subsurface setting. The emerged carbonate platform drowned during the middle early Valanginian as a result of eustatic sea-level rise and tectonic subsidence and was covered by Valanginian turbidites. During a second, more intensive period of tectonic deformation, probably in the late Valanginian, the development of large rotational faults resulted in tilting of the carbonate platform blocks toward the east. After tilting, the outer margin rapidly subsided to abyssal depths during the Late Cretaceous-early Tertiary. The development of the carbonate platform helps in dating the major tensional episodes on the western flank of Galicia Bank as late Berriasian-earliest Valanginian and ?late Valanginian in age.

INTRODUCTION

The depositional and tectonic history of the Late Jurassic carbonate platform on the western side of Galicia Bank is presented in this contribution. The results of our study have provided new evidence about the tectonic evolution of the Galicia margin and have advanced our understanding of the paleogeography of the northern central North Atlantic during the Late Jurassic-Early Cretaceous.

This chapter is divided into two parts. The first, analytical part provides a detailed petrographic description of the sedimentary rocks encountered. The second part is data interpretation, a discussion of paleoenvironment, diagenesis, dolomitization, tectonics, and paleogeography.

The objective of Ocean Drilling Program (ODP) Leg 103 was to resolve the geologic and paleoceanographic history of the Galicia margin (Fig. 1A) in relation to the rifting and continental separation between the Iberian and eastern North American continental plates. A multiple reentry hole was located on regional seismic line GP-101 (Fig. 1B) and designated as ODP Site 638 (Fig. 1C). The site was located near the upper part of the upward tilted edge of the rotated tectonic block to ensure sampling of a complete Mesozoic stratigraphic succession from rifting phases, through the drowning of the carbonate platform, to changes in the environment during plate separation as the margin thermally subsided to oceanic depths.

The finding of Lower Cretaceous terrigenous turbidite beds beneath seismic reflector 4 (Fig. 1C), previously identified as the top of the pre-rift carbonate platform sequence at Site 638 (Mougenot et al., 1985; Boillot, Winterer, et al., 1987), required major revision of the existing seismic interpretation. Drilling difficulties in the Lower Cretaceous turbidite sequence at this site led to the abandonment of the hole without reaching the deep objective.

Shipboard reassessment of the seismic data showed that the carbonate platform could be reached about 3 km to the west of Site 638, where it possibly could be exposed at the fault escarpment, covered by a thin veneer of Cenozoic sediments. Thus, Site 639 was established to drill through the carbonate platform into underlying basement rocks (Fig. 1C). Technical difficulties in drilling the carbonates forced premature abandonment of Hole 639A after penetrating only 89.8 m below seafloor (mbsf). In an effort to reconstruct the stratigraphy of the carbonate platform, another five holes were drilled in an east-west transect about 800 m long, downdip of the escarpment (Fig. 2) (Shipboard Scientific Party, 1987b). The reason for this six-hole transect was that none of the holes was able to penetrate into the carbonates by more than few cores before the drill pipe would become stuck, forcing abandonment of the hole.

Drilling operations at Site 639 provided only fragmentary data about the carbonate platform and its history (Shipboard Scientific Party, 1987b). The incomplete stratigraphic record together with poor core recovery (about 20% in Holes 639A through 639D and less than 5% in Holes 639E and 639F) resulted in an uneven sample coverage for reconstruction of the carbonate platform depositional history.

¹ Boillot, G., Winterer, E. L., et al., 1988. *Proc. ODP, Sci. Results*, 103: College Station, TX (Ocean Drilling Program).

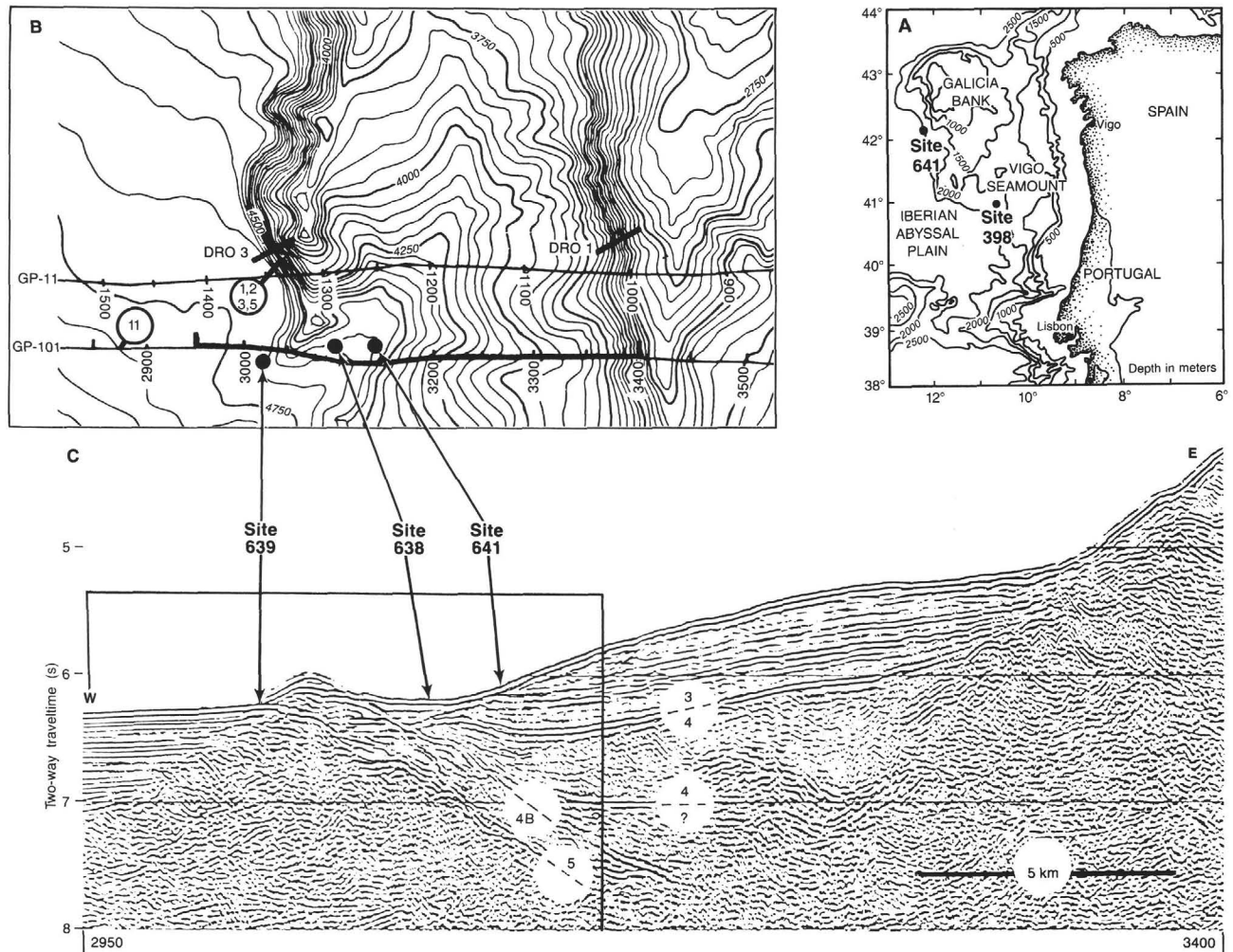


Figure 1. **A.** Location of Site 639 on the Galicia Bank. **B.** Sea Beam map of the area with locations of Site 639, seismic sections, and dredge stations. Note that the tectonic structure is mimicked in the seafloor morphology with the upward-tilted edges of the half-grabens forming steep escarpments at the sea bottom. The two dredge stations on these escarpments are DRO1 and DRO3. Approximate locations of submarine dives (Boillot et al., this volume) are marked by circled numbers. **C.** Multichannel seismic-reflection line GP-101 with plotted location of Site 639. The numbers on the line correspond to the seismic data interpretations prior to drilling (Mougenot et al., 1985; Boillot, Winterer, et al., 1987). According to this interpretation, seismic Unit 5 corresponds to the pre-rift sequence, Unit 4 to syn-rift, and Unit 3 to post-rift strata. It was assumed that the top of the carbonate platform corresponded to seismic reflector 4B. Frame outlines portion of seismic line geologically interpreted in Figure 2.

The Shipboard Scientific Party (1987b) proposed two possible interpretations for the seismic section across Site 639. In this paper we support and modify the normal-fault interpretation (Fig. 47 of the Shipboard Scientific Party, 1987b) for the seaward edge of the carbonate platform. That interpretation implies that drilling a transect across the buried carbonate escarpment may not provide a complete stratigraphic section through the platform (Fig. 2).

Considering the poor core recovery, the interpretation of the Mesozoic carbonate platform that we provide in this paper is generalized and subjective. It is based on core and thin-section studies, geophysical logs, and seismic-reflection data. The known evolution of synchronous carbonate platforms in northern Spain, Portugal, and the Grand Banks and the results of dredging on the western Galicia margin (Dupeuble et al., 1987) assisted in reconstructing the geologic history of the Galicia Bank carbonate platform.

We dwell only briefly on limestone diagenesis and dolomitization, the subjects of other contributions in this volume (Loreau and Cros; Haggerty and Smith; Daniel and Haggerty). The biofacies study of the limestones by Moullade et al. (this vol-

ume) complements our study. However, there is major difference between our and Moullade et al.'s studies in that the latter authors used as a working hypothesis the early concept of the shipboard party (Fig. 27 of Shipboard Scientific Party, 1987b), according to which the holes tested progressively deeper stratigraphic horizons of the carbonate platform down to the underlying basement. This difference in concept of tectonic setting results in different interpretations not only of the carbonates but also of the tectonic evolution of the whole region.

TECTONIC SETTING

Detailed discussion of the tectonic setting of the Galicia Bank can be found in the *Initial Reports* of Leg 103 (Boillot, Winterer, et al., 1987). Here, we concentrate only on the part relevant to the development of the carbonate platform. Site 639 is on the uplifted, outer flank of a tilted block (Fig. 1C). The section dips to the east and subcrops on a westward-sloping submarine erosion surface, now buried under an overlapping wedge of Upper Cretaceous and Cenozoic pelagic sediments. The top of the carbonate platform is overlain unconformably by Valanginian pelagic sediments.

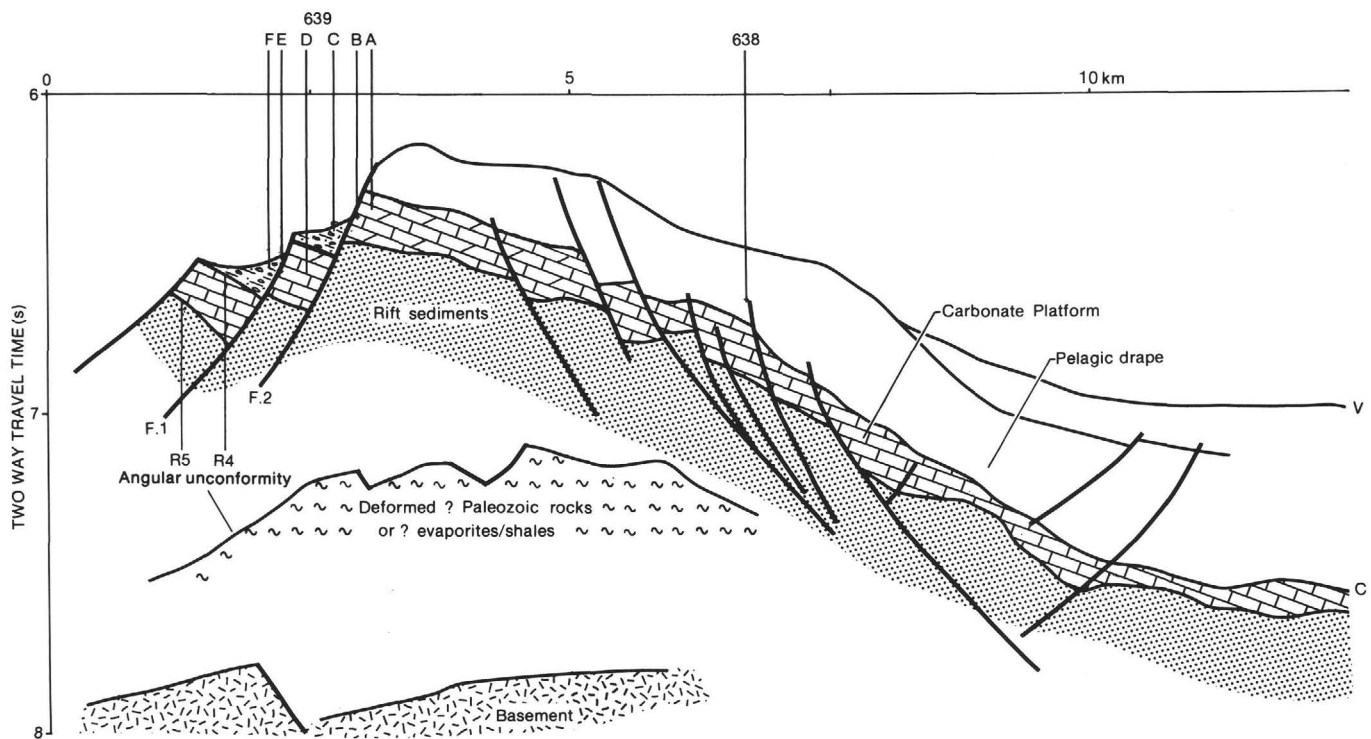


Figure 2. Geologic interpretation of the segment of seismic line GP-101 shown in Figure 1C, demonstrating the tectonic setting of the carbonate platform near Site 639 and position of drill holes. Seismic reflector C corresponds to the top of carbonate platform; reflector V to an untested clastic unit of probable Hauterivian age.

Reinterpretation of the seismic-reflection profile across Site 639 (Fig. 2) shows that the outer edge of the carbonate platform is highly broken by synthetic and antithetic faults. Faulting resulted in downthrown blocks to the west, with rotation along listric faults. Small tectonic troughs produced between the fault blocks acted as catchment basins for the upslope-derived detritus.

The carbonate platform seems to thicken to the west, with the thickest section near the escarpment edge where the seismic thickness reaches approximately 0.17 s (Fig. 1). Applying an average compressional seismic velocity for carbonates of 4.7 km/s (Shipboard Scientific Party, 1987b), the thickness of platform could be up to 420 m. However, because the platform is inhomogeneous from intercalation of clastics, the thickness is possibly less. The strong seismic reflector at the base of the outermost downfaulted block points to separation of the carbonate platform from the underlying rocks by an unconformity. The seismic data do not adequately resolve the character of the rocks underlying the carbonate platform. The character of the seismic sequence below the carbonate platform could indicate that it is either of sedimentary origin or is composed of low-grade meta-sedimentary rocks. The thickness of this basal sequence, underlain by a weak reflector, is approximately 1400 m (assumed compressional velocity of 4 km/s). Such an interpretation seems to find support in the results of submersible dives along the Galicia margin (Boillot et al., this volume). Dives on the escarpment 6 km to the north of the drill site documented the presence of about 500 m of sedimentary rocks that are older than those recovered at Site 639. This sequence is composed of intercalated clastics and dolomites, with dolomites near the base. The age is unknown but is possibly Mesozoic. The sediment sequence overlies weakly metamorphosed sedimentary rocks intercalated with volcanoclastics of probable Paleozoic age (Boillot et al., this vol-

ume). The strong reflector that occurs at 8 s two-way traveltime (tw) below seafloor on seismic line GP-101 near the drill site (see Mauffret and Montadert, this volume) we interpret as corresponding to the top of the crystalline basement (Fig. 2).

Combining the results of seismic data interpretation, drilling, and studies of thin sections, we have concluded that Hole 639A was drilled at the top of the block-faulted carbonate platform (Fig. 2). Hole 639B was probably drilled into the same tectonic block but encountered a deeper stratigraphic level than Hole 639A. Hole 639C is situated in one of the tectonic grabens between rotated limestone blocks and thus, recovered debris derived probably from the upslope exposure of basement. We suggest a similar origin for the polymictic debris of clastics, carbonates, and basement rocks encountered in Holes 639E and 639F, which are in a similar tectonic depression but below the next downslope rotated limestone block. Hole 639D was probably drilled into one of these limestone blocks and provides the only stratigraphically continuous section of the carbonate platform. However, the carbonate platform was not penetrated in its entirety at this site.

CARBONATE PLATFORM

Holes 639D, 639B, and 639A have been used to reconstruct a composite stratigraphic section of the carbonate platform (Fig. 3). The limestones in Holes 639A and 639B are completely dolomitized; in Hole 639D only the top is dolomite. For descriptive purposes, we retained the general lithologic framework subdivision established by shipboard study (Shipboard Scientific Party, 1987b). The Valanginian marlstones overlying the carbonate platform at Hole 639A correspond to Unit III, the underlying dolomites to Unit IV, and the limestones of Hole 639D to Unit V. The units are described in ascending stratigraphic order in the following text. The petrographic data for the limestones and do-

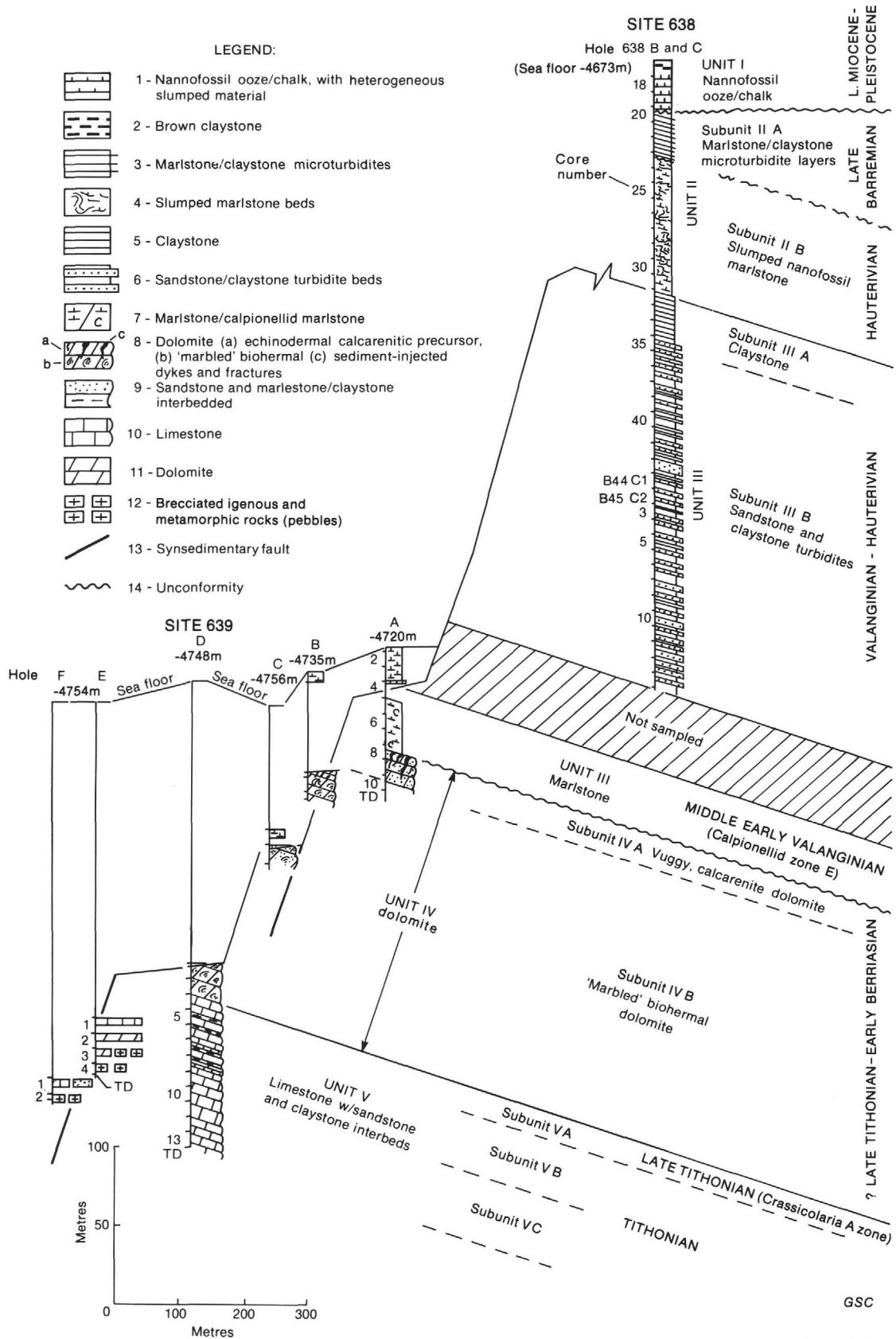


Figure 3. Composite stratigraphic section of Sites 639 and 638, showing schematic lithology and lithostratigraphic subdivision of drilled sedimentary strata. Water depths of each hole are in meters below sea level, as determined from echo-sounding profiles.

lomites are summarized in geologic charts (Fig. 13), which are similar to those published for Jurassic limestones off Morocco by Jansa et al. (1984).

Unit V

Unit V, composed of limestones and intercalated clastics, was encountered in Hole 639D. The thickness of the penetrated sequence is 94.1 m. Three subunits are recognized on the basis of changes in lithological composition (Shipboard Scientific Party, 1987b): the basal Subunit VC is characterized by the occurrence of oncolith-skeletal wackestones and packstones; Subunit VB consists of mixed terrigenous sandstone-marlstone and fine-grained limestone lithologies; and the upper Subunit VA is biohermal limestone beds intercalated with marlstone and skeletal-peloid wackestone containing planktonic biota. Each of the subunits includes a variety of microfacies, which we describe here in more detail.

Subunit VC: Large Foraminifer-Oncolith Limestone Lithofacies (base of Core 103-639D-13R to top of Core 103-639D-9R)

The limestones in Subunit VC are light to brownish gray oncolithic wackestones and packstones and peloidal packstones, intercalated with a minor amount of gray, skeletal peloid wackestone to grainstone. Two thin beds of pale olive marlstone are intercalated with the limestone in Core 103-639D-10R. The marlstone is bioturbated and contains scattered foraminifers and rare serpulids. Limestones are fractured with hairline fractures filled by calcite. Stylolites are commonly oriented parallel to bedding planes; locally, development of horsetail stylolites results in a pseudobrecciated limestone texture. The intensity of pressure solution is demonstrated by the juxtaposition of very different lithologies on each side of the stylolite, as seen in Section 103-639D-13R-2. Concentration of iron oxides along some of the stylolite seams suggests that the stylolitic seams were passageways for the migration of oxygen-rich fluids.

Microfacies Description

Oncolith-Skeletal-Peloid Wackestone to Packstone Microfacies. Packstone is the most common textural type in Subunit VC and consists of a mixture of oncoliths, skeletal debris, peloids, and micrite. The most characteristic feature of these rocks is their grain size bimodality (Fig. 4A). The coarse fraction is composed of oncoliths 0.1 to 4 mm in diameter, averaging about 2 mm in diameter. The second, finer fraction is of fine-sand-size peloids. Oncoliths (1%–40%) are scattered throughout the sediment and are only rarely concentrated in thin laminae. The oncoliths have nuclei composed of skeletal particles (larger foraminifers, algal debris, and mollusk debris), composite grains, micrite, or sparry calcite, which fills a cast in replacement of dissolved skeletal debris. Sessile foraminifers locally overgrow the oncoliths. The finely laminated texture of the original algal coatings is rarely preserved. Almost all of the oncoliths show a high degree of micritization, which mostly affected the outer envelopes, thereby giving the appearance of a massive micrite rim (Fig. 4B).

Peloids are the other dominant component of this microfacies, accounting for up to 50% of the sediment. The peloids are 0.07 to 0.25 mm in diameter, rounded to oval in shape, with a well-defined boundary (Fig. 4A), and were of a hard type. Ghosts of a skeletal fabric are observed in the center of some larger peloids, which suggests that some of them are micritized skeletal debris. Others, particularly the oval-shaped larger peloids, could be fecal in origin. Fossil remains (up to 10%) are dominated by large benthic foraminifers, *Anchispirocyclina lusitanica* and Lituolidae (Moullade et al., this volume); less common are small benthic foraminifers (*Trocholina* and *Lenticulina*), echinoid spic-

ules, gastropods (*Nerinea*), ostracodes, and mollusk debris. Some dasycladacean algae debris is also observed (Fig. 4C). Traces of calcisponges, corals, and hydrozoans are also found in this subunit. The allochems are enveloped by micrite. From the lower part of Core 103-639D-11R to the base of the drilled sequence, the micritic matrix shows crystal enlargement (Fig. 4D), in which the micrite is replaced by microspar. The molds from dissolved skeletal fragments and voids in some of the skeletal debris are filled by slightly ferroan, coarse, blocky sparry calcite. Dolomite occurs only in traces along some of the stylolitic seams and fracture fillings and also as reliefs in the matrix. Ghosts of dolomite rhombohedra suggest that minor dedolomitization occurred.

Skeletal-Peloid Packstone Microfacies. This microfacies is found mainly in the upper part of Subunit VC (Cores 103-639D-9R to 103-639D-11R; Fig. 3), where it is intercalated with the oncolith-skeletal-peloid packstone microfacies. The only difference between these two microfacies is that this one lacks oncoliths. Small foraminifers (valvulinids and *Trocholina*) and mollusk and dasycladacean algae debris are the recognizable biota in the packstones. In some of the packstones, the peloids were merged by compaction, which gives the rocks an appearance of being dominantly micrite. However, closer examination reveals the original peloid nature of the sediment. The merged peloid texture indicates that these peloids were of a soft type and that lithification had to occur relatively early. The peloids are of a different origin than the "hard" peloids of the oncolith microfacies.

Fossiliferous Micrite Microfacies. Except in Section 103-639D-10R-1, this microfacies is otherwise only a minor component of Subunit VC. Silt- to fine-sand-size bioclast debris represented by large foraminifers, thick-walled mollusk shells, gastropod and dasycladacean algae debris, and serpulids (Figs. 4E and 4F) is surrounded by a matrix of micrite, with traces of quartz silt and clay. The generally finer-grained texture of the limestones in Cores 103-639D-10R and 103-639D-9R and the appearance of marls in Core 103-639D-10R are indicative of a transitional boundary between Subunits VC and VB and of a decrease in energy conditions.

Subunit VB: Mixed Terrigenous Clastics-Limestone Lithofacies (Cores 103-639D-8R through 103-639D-6R)

Light gray, light yellowish brown to light reddish brown fine-grained limestones are intercalated with about 20-cm-thick beds of light yellowish brown silty marlstone, silty calcareous clay, and olive-colored clay. Intercalations of a coarse-grained, yellowish brown sandstone and pale olive siltstone were sampled in Cores 103-639D-7R and 103-639D-8R (Fig. 5). The contacts between individual lithologies were generally not recovered, with the exception of some gradational contacts with marls in Cores 103-639D-6R and 103-639D-8R. Density and gamma-ray logs indicate that the sandstone beds are more common in this unit than is apparent from the coring results. The terrigenous beds on the geophysical logs are 1 to 2 m thick and alternate with 1- to 9-m-thick limestones. The limestones are of variable composition, with the most common type being sandy quartz or silty quartz skeletal-peloid packstone to wackestone (Fig. 6A). In minor abundance are skeletal wackestone, biomicrite, and skeletal-oncolith wackestone, along with rare occurrences of foraminiferal grainstone.

Macroscopic examination shows locally intensive stylolitization of the limestones. Bedding is not well developed, but in some of the marlstones, lamination is caused by the accumulation of large foraminifers into 5- to 20-mm-thick laminae (Fig. 5). These laminae have a 20° to 30° inclination that may be indicative of the magnitude of post-depositional tilting of the beds.

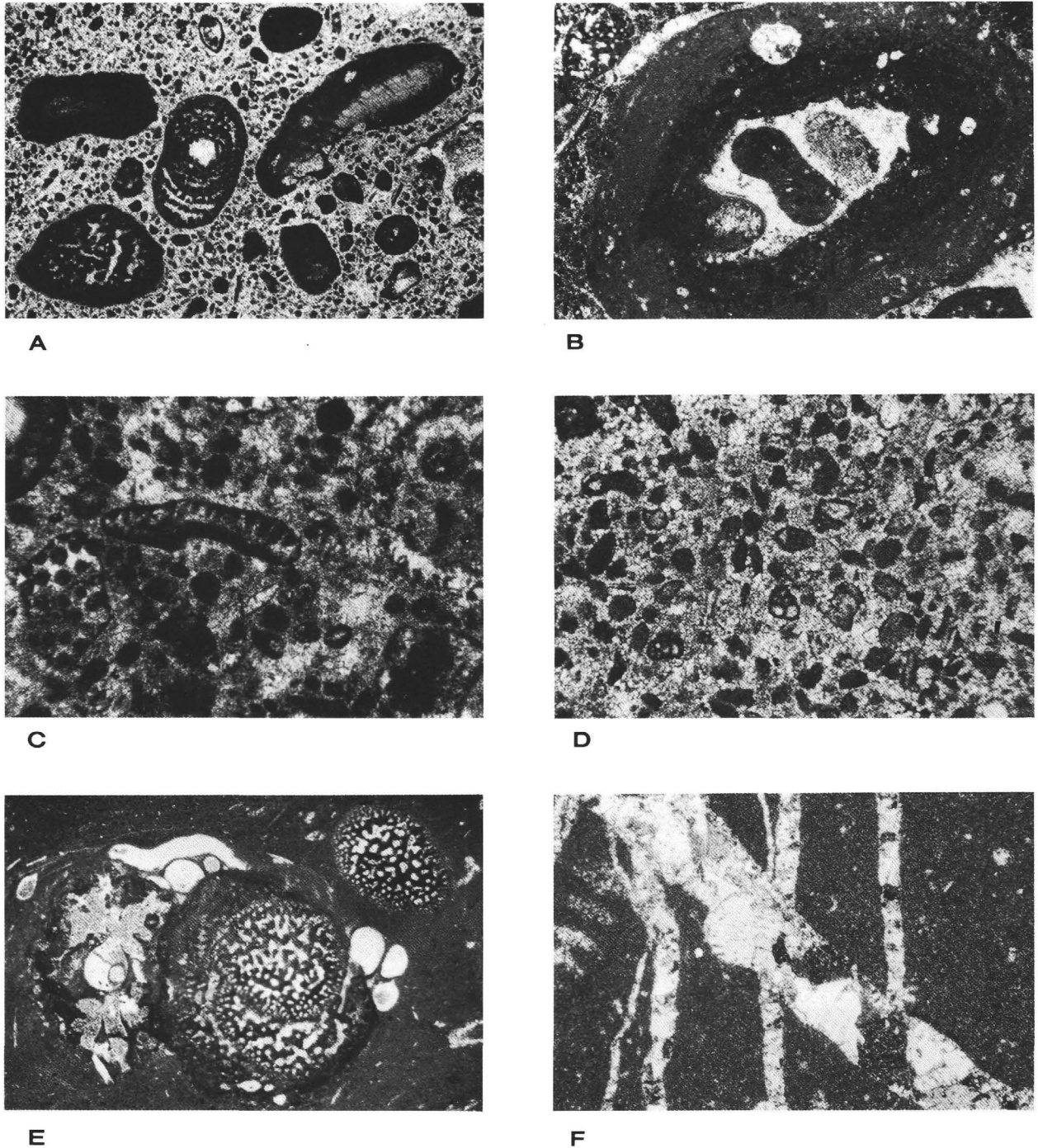


Figure 4. Thin-section photomicrographs of Subunit VA. **A.** Oncolith-peloid wackestone to packstone. Note the bimodality in size distribution of the particles. The coarse fraction consists of oncoliths that have nuclei of large foraminifers and mollusk and unidentifiable skeletal debris. The finer fraction is comprised of mostly subangular, less rounded, hard peloids. Sand-size bioclast debris and small benthic foraminifers (valvulinids) are less common. Crystal enlargement resulted in replacement of the original micrite matrix by microspar, which produced a pseudograinstone texture. Sample 103-639D-13R-1, 29 cm; ordinary light; scale bar = 1 mm. **B.** Detail of an oncolith showing the intensively micritized outer rim. Inside the oncolith the laminar character of the coatings around the gastropod nucleus is still recognizable. Sample 103-639D-13R-2, 72 cm; ordinary light; scale bar = 1 mm. **C.** Dasycladacean algae (*Linoporella* and *Epimastopora*) debris in an oncolith-peloid packstone. Sample 103-639D-12R-3, 56 cm; normal light; scale bar = 0.2 mm. **D.** Well-sorted skeletal-peloid packstone. Small foraminifers dominated by valvulinids are common; other skeletal debris is poorly preserved and micritized. Hard peloids are mostly subangular in shape. Micritic matrix has been replaced by microspar. Sample 103-639D-11R-2, 45 cm; ordinary light; scale bar = 0.5 mm. **E.** Large foraminifer encrusted by serpulids in biomicrite. Fragments of algae occur at lower left. Sample 639D-10R-1, 74 cm; crossed nicols, scale bar = 1 mm. **F.** Biomicrite cut by two diachronous sets of sparry calcite-healed fractures that intersect at a 45° angle. Sample 103-639D-10R-1, 128 cm; normal light; scale bar = 1 mm.

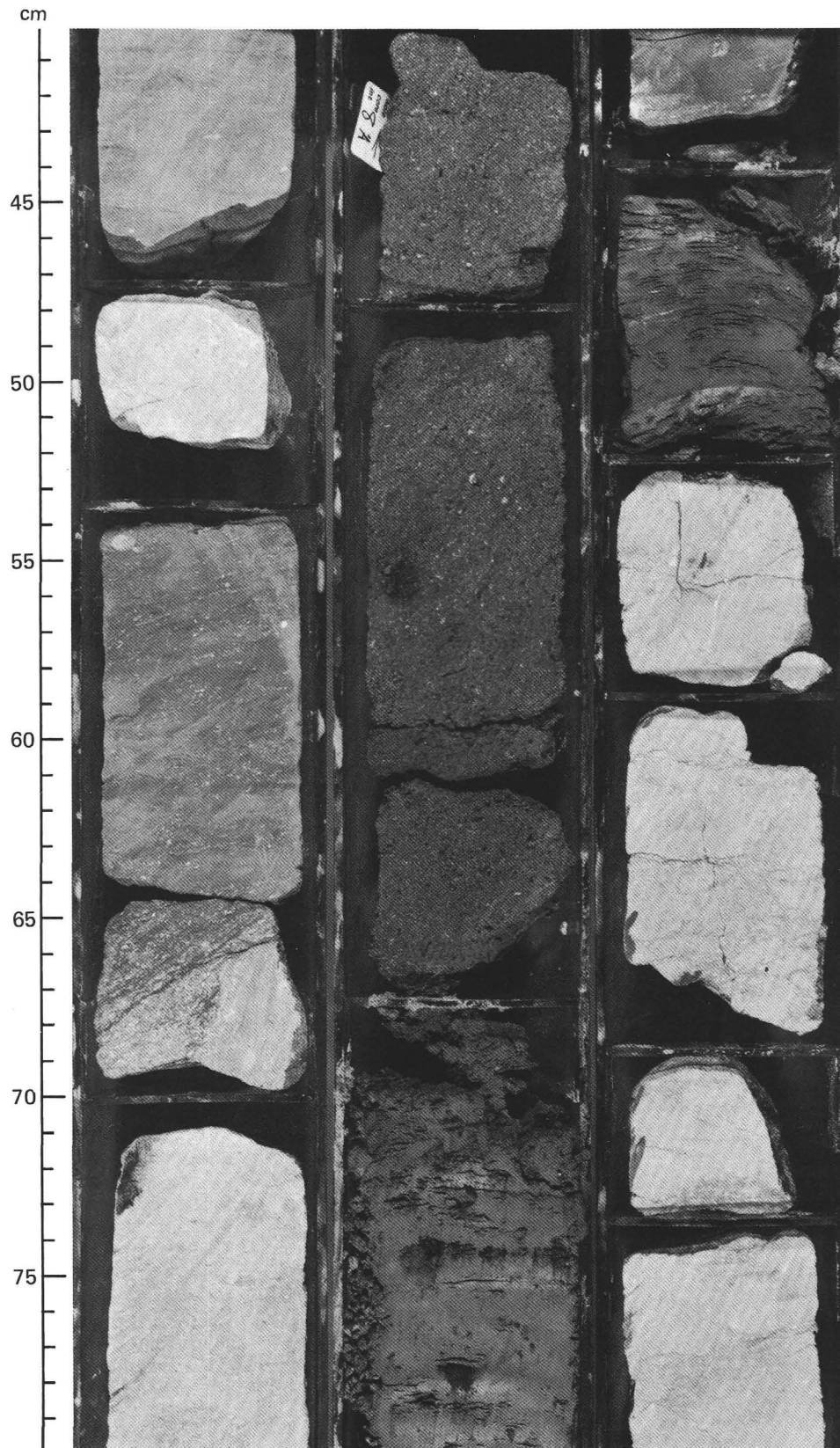


Figure 5. Typical lithology of Subunit VB. Clayey limestones alternate with beds of marlstone and medium- to coarse-grained sandstone in the 40–80 cm interval of Sections 103-639D-7R-1, 103-639D-7R-2, 103-639D-7R, CC, and 103-639D-8R-1.

Microfacies Description

Sandy Quartz and Silty Quartz Limestone Microfacies. A distinct feature of this microfacies, other than the presence of terrigenous components, is the occurrence of a broad variety of small benthic foraminifers. Particularly common are epistominids and litulidae; lagenids, miliolids, and valvulinids are rare. *A. lusitanica* is present in the skeletal-oncolith wackestone microfacies, which is similar to that in Subunit VC, and was found to be present in all Subunit VB cores. Of the other biota, gastropods and thick-walled mollusks are common. Algae debris is a minor constituent (Fig. 6B), dominated by dasycladacean algae (up to 5% in some cores), with *Cylindroporella*, *Salpingoporella annulata*, and *Zergatella* identified. Also occurring are Cyanophytae (*Girvanella* type and spongiostromata), which coat bioclasts and construct incipient stromatolite-like growth structures (Fig. 6C). Annelid, echinoid, and ostracode debris is rare, and coral, calcisphere, and calpionellid debris is found in trace amounts. Algal oncoliths about 3 mm in diameter are a minor component of a skeletal-peloid limestone in Cores 103-639D-6R and 103-639D-8R. Oncoliths in Core 103-639D-8R have an irregular outline coated by iron-manganese film, which is indicative of a brief period of nondeposition and solution, most probably as a result of a periodic influx of fresh water. Strong micritization of bioclasts in the mixed carbonate/terrigenous clastics microfacies also suggests alteration resulting from fresh water. Silt-size peloids and micrite (which has been locally recrystallized into microspar) plus minor clays and quartz silt to fine-grained sand form the matrix of the packstones and wackestones.

Foraminiferal Grainstone Microfacies. This microfacies was recovered in Sample 103-639D-7R-1, 71–75 cm. The grainstone is well sorted and reversely graded. The most common grains are rounded or lightly coated debris of large foraminifers (15%–20% *A. lusitanica*), worn mollusk and gastropod debris (some pieces of which were micritized and encrusted by sessile foraminifers), poorly preserved red algae (*Lithothamnium*), and dasycladacean algae (*Cylindroporella*). Minor components are fine quartz grains and rounded micrite intraclasts, all cemented by patchy, sparry-microsparite calcite (Fig. 6D). Grainstone is a rare microfacies not only in Subunit VB but in all of Unit V.

Terrigenous Sediments. All types of gradations between clean carbonate, marl, and calcareous to terrigenous sand are found in Subunit VB. In the marl, clay input dilutes the carbonate without observably changing its texture. Concentrations of larger foraminifers into laminae in the marls indicate redeposition, current transport, and mixing of sediment from two sources.

Terrigenous sandstones are fine- to medium-grained and mostly poorly sorted, with grains angular to subangular in shape (Fig. 6E). The dominant constituent is quartz, with feldspars as a minor component (6% to 16%). The feldspars range from fresh to almost completely kaolinized. Plagioclase is the most common, with microcline and orthoclase less common. Chert, sericitic quartzite, metamorphic quartz, chloritized biotite, and muscovite are the other minor constituents of the sandstone. Felsic igneous rock fragments occur in trace amounts. Of special significance for clastics provenance determination is the clast of feldspathic rock in the sandstone of Section 103-639D-7R-2. The feldspars in this lithoclast have a radial fibrous texture, similar to that found in “basement” rock fragments in Section 103-639F-2R, CC. Some of the feldspathic sandstones (Section 103-639E-7R-2; Fig. 6E) lack carbonate grains, have an argillaceous matrix, and are cemented in part by coarse dolospar. Other feldspathic sandstones (Section 103-639E-8R-2) are better sorted and contain up to 10% carbonate allochems composed of rounded sand-size clasts of micrite, rare worn mollusk debris, larger foraminifer tests (Fig. 6F), micrite-coated quartz grains, and a few

micritized oolitic grains cemented by blocky, low-iron sparry calcite.

Subunit VA: Biohermal Limestone Lithofacies (Cores 103-639D-5R through 103-639D-4R)

Geophysical logs indicate that this subunit consists of about 4 m of well-lithified limestone, which was penetrated by Core 103-639D-5R, overlain by a marlstone with another 1-m-thick limestone found in Core 103-639D-4R. However, only 3% of Core 103-639D-4R was recovered, consisting of pieces no larger than 6 cm of limestone of varying colors and lithologies. This may indicate that the limestone in Core 103-639D-4R is a breccia from the exposed limestone escarpment above, but it may also reflect the lithologic variation of the strata. No soft sediment, which may have separated limestone beds, has been recovered; thus, it remains unknown whether the limestone in Core 103-639D-4R is an autochthonous or allochthonous debris deposit. The similarity in composition between the limestones in Cores 103-639D-4R and 103-639D-5R and regional considerations lead us to consider the limestones to be autochthonous deposits. Because only fragments of variable composition were recovered, we have not divided this subunit into microfacies.

The limestone in Core 103-639D-5R consists of fragments of a hydrozoan floatstone, framestone, and rudstone (Figs. 7A through 7C) intercalated with intraclast skeletal packstone, skeletal wackestone, packstone, and biomicrite. The biohermal limestone is fractured (Fig. 7C), with fractures filled by iron oxide-stained sparry calcite. The fauna of the biohermal limestone is a mixture of hydrozoans (*Parastroporoidea*), chaetetids (*Blastochatetes*; Figs. 7A and 7B), stromatoporoids (*Cladocoropsis mirabilis*), corals (*Stylamina* and *Pennulados*), bryozoans, and calcareous sponges. Several stages of encrustation by *Girvanella*, *Thaumatoporella*, *Lithocodium*, and microbial crusts can be recognized on surfaces of some of the hydrozoans (Fig. 7A), suggesting multiple encrustations and organic binding of frame-building biota. The debris of a frame-building biota were deposited in bioturbated, silt-size fossiliferous-peloid carbonate muds, with echinoids, mollusk debris, and benthic foraminifers (Fig. 7B) as additional skeletal carbonate constituents.

The biohermal limestone is intercalated with a skeletal-peloid wackestone and packstone similar in composition to that forming the “matrix” of the biohermal limestone. Preservation of geopetally filled borings in the skeletal-peloid wackestone (Sample 103-639D-5R-3, 42 cm) requires early lithification. A cryptalgal, clotted structure resembling a thrombolite in a fragmented skeletal-peloid packstone was observed in Sample 103-639D-5R-2, 95 cm (Fig. 7E). Such features are occasionally found to grow between skeletal debris in the reef flank deposits in a deep subtidal environment. The accumulation of algal debris, belonging to Solenoporacea (*Thaumatoporella*), Gymnocodiacea (*Permolcalculus*), and Codiaceae (*Arabicodium*, *Lithocodium agregatus*, and *Bacinella irregularis*) (Sample 103-639D-5R-3, 34–43 cm) contrarily indicates a shallower depositional environment, unless the algal debris was retransported. As a diagenetic curiosity, we note the occurrence of corals, replaced in part by coarse, zoned dolospar and silica (Sample 103-639D-5R-2, 75–77 cm).

As no samples were available for study of the 10-cm-thick bed of olive silty clay intercalated with the limestones at 40–50 cm in Section 103-639D-5R-1, the composition and origin of this bed is unknown.

At the top of Subunit VA, the limestone is pale, yellowish brown and pink, skeletal peloid wackestone and biomicrite. The individual core pieces recovered are not larger than 6 cm long and are rather rounded. Fauna recognizable in this limestone includes unsorted sand-sized debris of mollusks, gastropods, bryo-

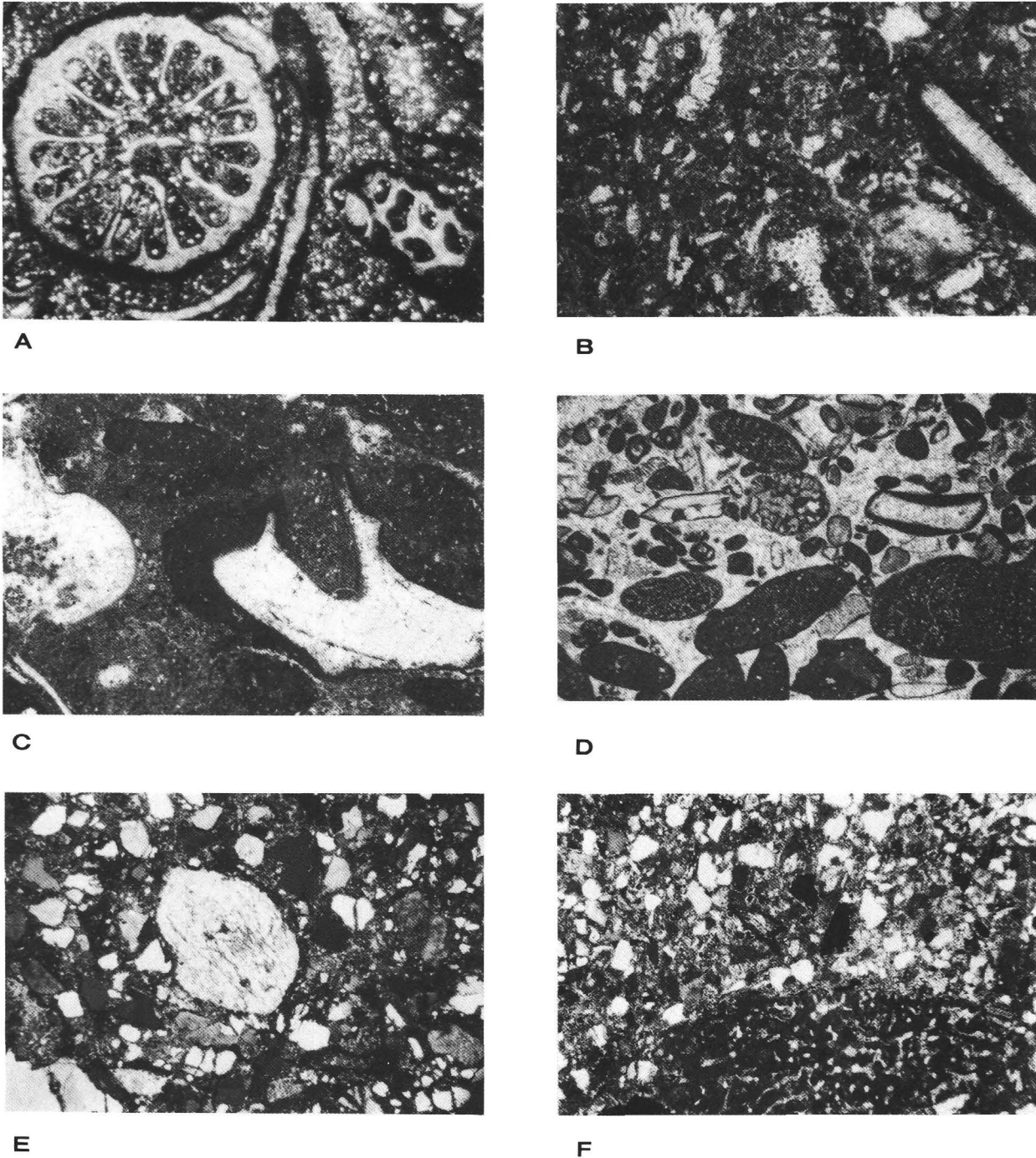


Figure 6. Thin-section photomicrographs of Subunit VB. **A.** Quartz silty skeletal wackestone. Holothurian plate in center. Mollusk debris and epistominids are coated by thin micritic envelopes and surrounded by a peloid, quartz silt, micrite matrix. Sample 103-639D-8R-1, 25 cm; normal light; scale bar = 1 mm. **B.** Unsorted skeletal packstone with common, small benthic foraminifers (*Epistomina*) and dasycladacean algal debris. This sample also contains a preserved fragment of *Permocalculus*. Oncolith with a mollusk fragment nucleus occurs at the top of view. Sample 103-639D-6R-1, 60 cm; ordinary light; scale bar = 0.5 mm. **C.** An algal stromatolite began to develop as an overgrowth on a gastropod fragment. The rest of the limestone is a skeletal wackestone with merged silt-size peloids and an argillaceous micrite matrix. Sample 103-639D-6R-1, 90 cm; ordinary light; scale bar = 1 mm. **D.** Foraminiferal grainstone. The dominant skeletal components are large foraminifers (*Anchispirocyclus lusitanica*) and a minor amount of abraded, thick-walled mollusk shell fragments cemented by sparry calcite. Note the reverse grading in the sediment. Sample 103-639D-7R-1, 71 cm; ordinary light; scale bar = 1 mm. **E.** Unsorted, medium-grained feldspathic sandstone with grains mostly subangular to angular in shape. Feldspars show a variable degree of alteration. The large orthoclase grain in the center is sheared and slightly kaolinized. The sandstone matrix is argillaceous with dolospar cement. Sample 103-639D-7R-2, 53 cm; polarized light; scale bar = 0.5 mm. **F.** Large foraminifer test and micrite intraclasts in a fine-grained calcareous sandstone. Sample 103-639D-7R-1, 34 cm; normal light; scale bar = 0.5 mm.

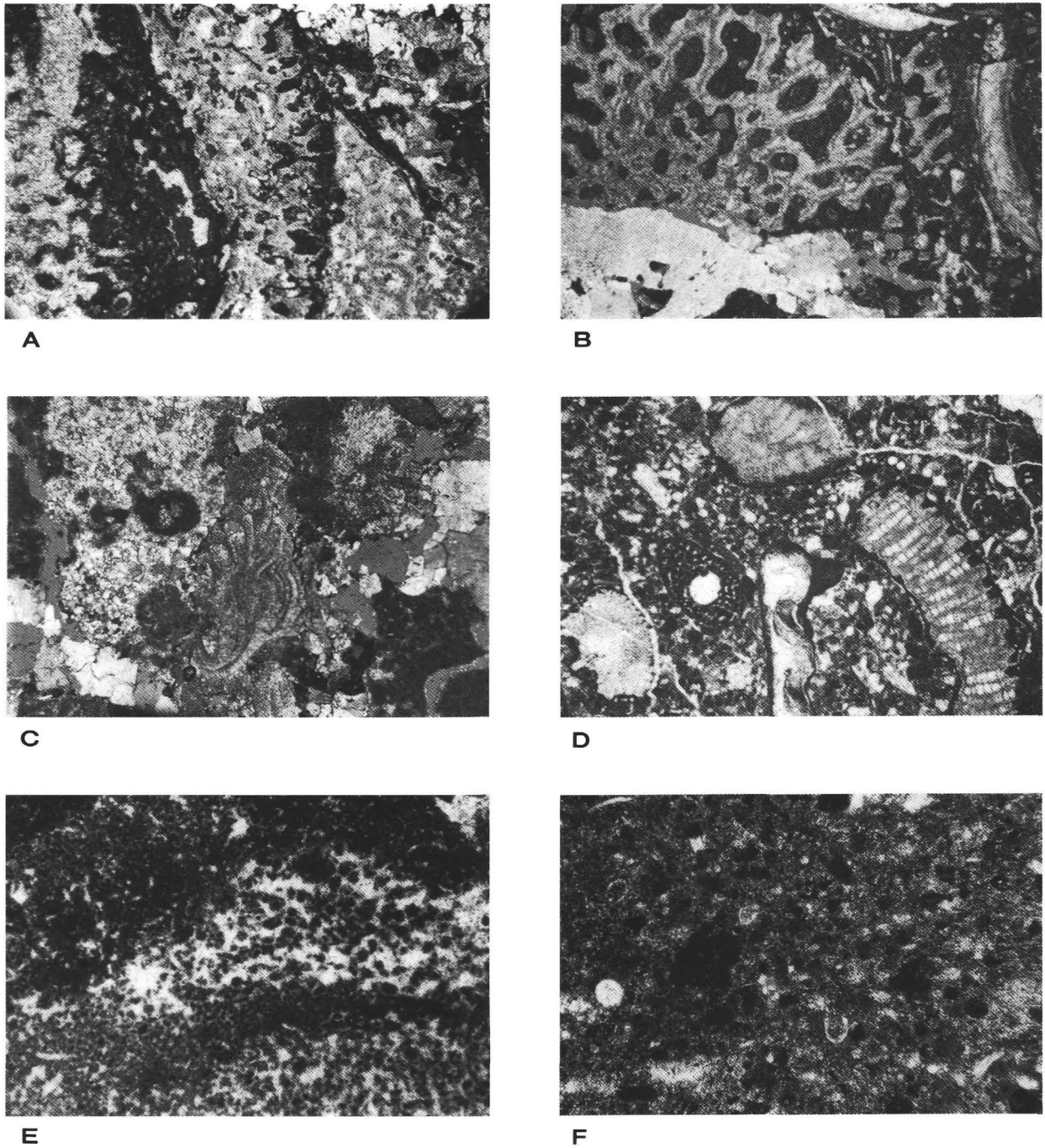


Figure 7. Thin-section photomicrographs of Subunit VA. **A.** Framestone formed by a complex overgrowth of hydrozoans and algae. A coral fragment is overgrown by the alga *Bacinella irregularis*, which is in turn coated by a rim of *Thaumtoporella porovesiculifera*. This latter alga is overgrown by chaetetids (*Shugraia*) encrusted by *Lithocodium*, which formed a substratum for a new colonization by chaetetids. Sample 103-639D-5R-3, 42 cm; ordinary light; scale bar = 0.5 mm. **B.** Breccia of biohermal limestone, composed of clasts of chaetetids, thick-walled mollusk shell fragments, echinoids, and calcisponges (the latter component not photographed). Fractures are healed by coarse, blocky sparry calcite. Sample 103-639D-5R-3, 34 cm; polarized light; scale bar = 0.5 mm. **C.** Breccia of biohermal limestone. Skeletal debris is replaced by coarse sparry calcite, with silt-size peloids accumulated in interparticle voids. An unidentified encrusting alga is in the center of the photograph. Sample 103-639D-5R-3, 34 cm; polarized light with gypsum plate; scale bar = 0.5 mm. **D.** Unsorted skeletal-peloid packstone with fragments of algal-coated corals, mollusks (note the development of the stromatolite in the center of the photograph), echinoids, large foraminifers, sand-size skeletal debris, and peloids. The lithified rock is fractured, with hairline fractures healed by sparry calcite. Sample 103-639D-5R-3, 13 cm; ordinary light; scale bar = 0.5 mm. **E.** Cryptalgal structure of a "deep-water" thrombolite. Spongiform microstructure resembling *Spongiostromata* consists of silt-size micrite clots. Filamentous texture is visible at the right upper corner of the photograph. The denser laminae probable represent periods of interruption in the thrombolite growth. Similar structures are found to be associated with biohermal debris deposited on the lower reef flanks. Sample 103-639D-5R-2, 95 cm; ordinary light; scale bar = 0.5 mm. **F.** Silt-size peloid wackestone with debris of ostracode and calpionellid tests. Preservation of the fragile shells indicates a low-energy depositional environment and pelagic influence on deposition. Sample 103-639D-5R-1, 105 cm; polarized light, scale bar = 0.2 mm.

zoans, echinoids, ostracodes, sponge spicules, and benthic foraminifers (lituloids). Larger foraminifers (*A. lusitanica*; Moullade et al., this volume) are also present. Scattered occurrences of calpionellids are common (Fig. 7F); coarse sand to pebble size fragments of corals, calcisponges, and hydrozoans are rare. Trace amounts of poorly preserved debris of red algae and algal oncoliths are also found. Allochems are deposited in a matrix of micrite and silt-size peloids. Geopetal fabric is well developed in Sample 103-639D-4R-1, 42–44 cm. The original voids, which could have been formed by the boring action of sponges, are partially filled by silt-size peloids, with the remaining part of the void filled by coarse sparry calcite.

Unit IV

The intervals from Sample 103-639D-4R-1, 10 cm, through Core 103-639D-2R in Hole 639D, Cores 103-639B-4R through 103-639B-2R in Hole 639B, and Cores 103-639A-10R through 103-639A-8R in Hole 639A consist of dolomite. From the interpretation of seismic data and lithologic appearance, we divide the dolomites into a brown marbled dolomite (Subunit IVB) recovered in Hole 639B and stratigraphically correlated for Hole 639D and a stratigraphically younger, light-colored sucrosic dolomite (Subunit IVA) penetrated in Hole 639A (Fig. 3).

Subunit IVB: Brown Marbled Dolomite

The recovery of Subunit IVB dolomites in Hole 639D (Sample 103-639D-4R-1, 10 cm, through Core 103-639D-2R) was very low, with recovery rates of only 2% for Core 103-639D-2R and 9% for Core 103-639D-3R. Difficulties with core recovery in Hole 639D seem to be explained by the geophysical logs, which indicate that the carbonate bed present in each of the cored intervals is only 2 m thick, with the rest of the interval consisting of marls or clays. Based on this evidence and on the small fragment size of the recovered dolomite, the dolomite in Hole 639D could represent a dolomitized debris flow. However, because the soft sediment intercalated with the dolomite beds was not recovered, we can not exclude that the dolomite is an *in-situ* deposit.

The dolomite is yellowish brown and grayish brown, fine to coarse crystalline, and vuggy. About 7% of the irregularly shaped vugs are several millimeters in size and are scattered throughout the rock. Some of the vugs are partially infilled by milky white dolospar whereas others are empty. The dolomite is cut by white veins, up to 5 mm thick, which are also of dolomitic composition. The original limestone texture was completely obliterated by wholesale dolomitization. The thin sections show medium to coarsely crystalline, euhedral, mostly zoned dolomite crystals with abundant impurities (Fig. 8A). The zoned dolomite crystals have rhombic, turbid nuclei. Iron oxides are found as partial infill of some of the intercrystalline voids. The original limestone fabric can sometimes be recognized by ghost structures of echinoids, mollusk debris, rare calcisponges and hydrozoans, and/or bioclasts of enigmatic origin (Figs. 8B through 8D). Extensive syntaxial cement around echinoderm fragments is evidence that ample interparticle space was present during cementation, indicating low compaction and early lithification of the dolomite precursor.

A similar dark, grayish brown, massive dolomite with minor intraclast breccia zones and complex patterns of voids, void fillings, and fractures filled by internal sediment and cement is present in Hole 639B (Cores 103-639B-2R through 103-639B-4R). We consider it to be part of Subunit IVB. This dolomite is a comparatively low-porosity rock, with only a few, large primary open pores. Typically, the dolomite shows a translucent, "marbled" appearance. The color shades and irregular mottling are reminiscent of predolomitization structures. The rubbly appearance sometimes mimics a floatstone or rudstone precursor (see fig. 10 in the "Site 639" chapter; Shipboard Scientific Party,

1987b), whereas local bafflestone/framestone-like textures are reminiscent of *in-situ* building organisms. However, this inference is not well substantiated.

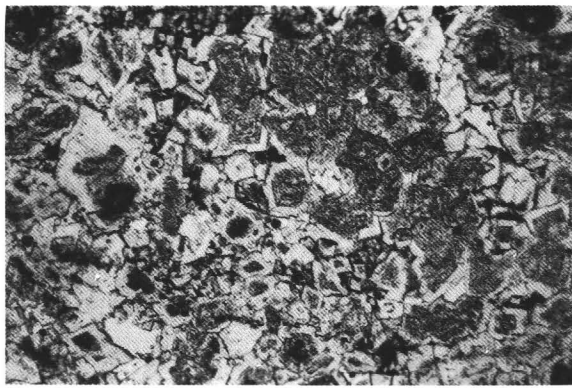
Dark, inclusion-rich dolomite is abundant in the thin sections and is accompanied by some clearer, inclusion-free dolomite (largely former calcite veins). Scattered echinoderm ossicles and ghosts of algae (dasycladaceans), foraminifers, bryozoans, gastropods, hydrozoans, and corals were identified in the dolomite, but patterns reminiscent of a much richer organic component remain largely unidentified. A distinctive feature of the marbled dolomite are flat, coupled "platy shells" of a thickness less than 1 mm, which have been previously referred to as phylloid algae (Fig. 11, "Site 639" chapter; Shipboard Scientific Party, 1987b). However, thin-section analysis did not confirm this interpretation. Downhole, where the dolomitization is less intense (Cores 103-639B-3R–103-639B-4R and 103-639C-2R), the dolomite is a lighter gray color and of a peloid-skeletal composition, with a varied biota (Fig. 8C) and local occurrences of solitary coral heads. Irregular tubules penetrating Sample 103-639B-4R-1, 98 cm, may indicate that this dolomite could have been part of a rhyzolith (Fig. 8D).

In the marbled dolomite, a multistage system of cavities and fractures documents complex multiple dolomitization, as we discuss subsequently. Both blocky dolomite (former calcite cement) and sediment are void-filling material. The sequence of void-filling events closely resembles that in the upper vuggy dolomite in Hole 639A. Cement alone is dominant in the smallest veins. The earliest recognizable features are irregular, wide voids, reminiscent of either primary interparticle voids of a coarse clastic deposit or open spaces within an organic framework. A later-formed system of fractures is superimposed and seems to crosscut the earlier structures. The geometric relationships between the earlier cavities and the crosscutting fractures are commonly obscured. Cavity formation and fracturing in the marbled dolomite predates the main dolomitization event, as documented by the crosscutting relationships between dolomite crystal boundaries and the fracture walls.

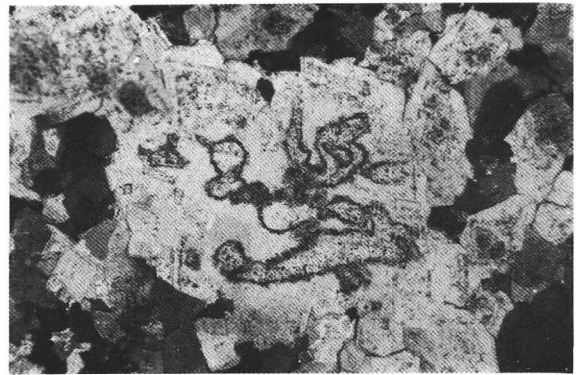
Subunit IVA: Light-colored Sucrosic Dolomite

Light brownish gray and yellowish brown, medium to coarse crystalline, sucrosic dolomite was recovered in Hole 639A (Section 103-639A-8R, CC, through Core 103-639A-10R). The original texture and composition of the limestones has been obliterated by extensive dolomitization, similar to that in Subunit IVB. Some ghosts of gastropods, bivalves, and echinoderms can be recognized. The other components are rounded bodies, 0.5 mm in diameter, that resemble the coated grains in Core 103-639D-9R. These occur together with echinoid debris, suggesting that the original carbonate was probably an echinoid-oid(?) skeletal grainstone and packstone.

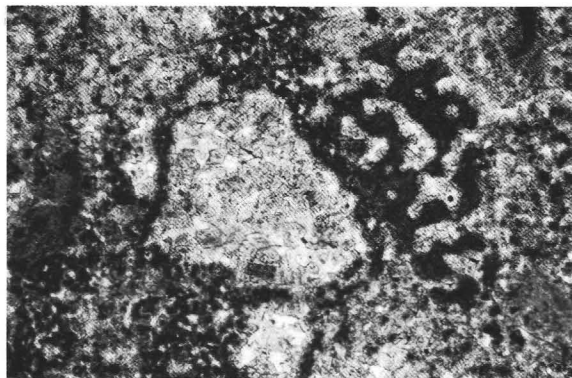
Open pores and sediment-filled and cemented cavities and fractures, as large as several centimeters in diameter, are notable features in the dolomite (see fig. 9 in "Site 639" chapter; Shipboard Scientific Party, 1987b). Locally, cavities and fractures are large enough to give the dolomite a brecciated appearance. Larger open cavities, reminiscent of fossil molds, are as much as 1–1.5 cm across. The smaller open pores are rounded in shape, average 1 to 3 mm across, and occur sparsely in most of the dolomite samples (birdseye-type structures?). Whatever their size, the open pores are lined by a single generation of drusy dolomite. These infilled cavities are roughly equidimensional or irregular in shape, or they display a sheetlike and/or vertical-fracture geometry. In the simplest case, void spaces are floored by a first generation of clear drusy dolomite, geopetally filled by internal sediment, and sutured by clear, blocky dolomite cement. Cavity-lining dolomite commonly displays a baroque habit (curved crystal faces and undulose extinction; Folk and Assereto, 1974).



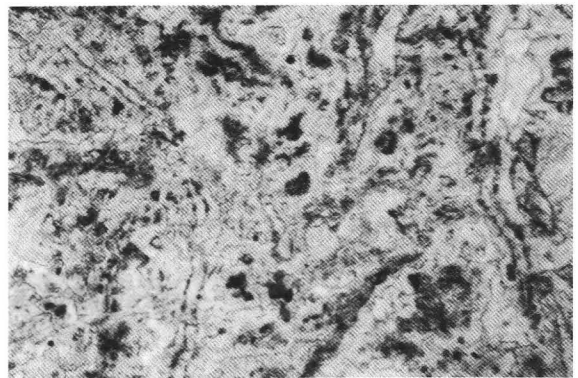
A



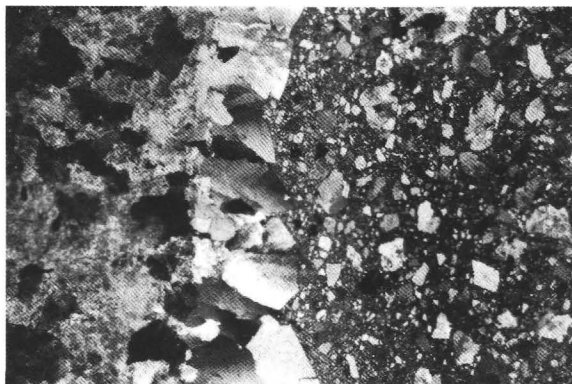
B



C



D



E



F

Figure 8. Thin-section photomicrographs of Unit IV. **A.** Medium crystalline dolomite with a complex dolomitization pattern. The dolomite precursor, probably an echinoid-oolitic packstone or wackestone, has been replaced by crystalline dolomite. Syntaxial rims of echinoids are replaced by clear dolomite. Other finer grained carbonate sediment particles or peloids are replaced by coarse dolospar with dirty nuclei. Larger clasts or voids were replaced (filled) by a patch of multiple-zoned coarse dolospar. After the period of leaching and solution, which produced enlarged voids and channel-type porosity, these were infilled by clear dolospar. The last stage was infiltration of iron oxide-stained clay sediment deposited in intercrystalline pores. Sample 103-639D-3R-1, 32 cm; ordinary light; scale bar = 0.1 mm. **B.** Coarse crystalline, poorly visible zoned dolospar with enclosed enigmatic tubiform structure in the center. Sample 103-639B-4R-1, 88 cm; polarized light; scale bar = 1 mm. **C.** Well-preserved ghost texture of calcisponge, micrite-coated intraclasts, and a ghost peloid texture replaced by coarse zoned dolospar in an original rock that was probably a biohermal limestone similar to that in the underlying core. Sample 103-639D-4R-1, 3 cm; ordinary light; scale bar = 1 mm. **D.** Medium crystalline dolomite, with interwoven net of tubules. Individual tubes, some branching, are bordered by a film of impurities. We interpret these as root casts. Rhyzolith is a reliable indicator of caliche and of subaerial exposure. Sample 103-639B-4R-1, 87 cm; ordinary light; scale bar = 1 mm. **E.** A fracture infilled by a mixture of unsorted broken fragments of dolomite crystals and dolomicrite. The wall of the fracture is rimmed by baroque dolomite. Note that the baroque dolomite crystals grow in an optical continuity with the dolomite crystals that were cut by the fracture. Sample 103-639B-4R, CC (12 cm); polarized light; scale bar = 1 mm. **F.** A fracture in the dolomite, infilled by dark dolomicrite and angular fragments of dolomite. The impure dolomite crystals and crystal zonation of the clasts in the fill is a clear documentation that this fracture was formed after the dolomitization of the limestones was completed. The fracture is rimmed by a discontinuous rim of clear dogtooth dolospar, which filled the remainder of the void after sediment compacted in the fracture. Sample 103-639A-10R-1, 81 cm; ordinary light; scale bar = 1 mm.

AGE OF CARBONATES

Baroque dolomite also is found lining fracture walls (Fig. 8E), and locally, it grows diagenetically at the expense of the internal sediment. Internal sediment in cavities chiefly consists of light gray, intraclast-rich peloid dolomiticrite, typically containing broken euhedral crystals of silt- and fine-sand-size dolomite. Crystal silt and a dolomite microspar mosaic, possibly replacing a primary crystal silt sediment, also occur as cavity fillings. Discrete laminae of dolomitic crystal silt and fine sand are interlayered with dolomitic micrite. Internal sediment layering indicates a multiple filling of the cavity. The presence of a cement crust between sediment laminae required that a certain amount of time elapsed before the following lamina was deposited. Laminations may suggest moderate current activity within caves or a storm-influenced bottom.

A late stage of randomly oriented to subvertical cracks, a few millimeters up to 1–1.5 cm wide, crosscuts the earlier formed structures. The fracturing is brittle and, based on the type of infilling material, we assign these features to two basic categories: (1) small-scale to microscopic, hairline cracks and veins, with a white sparry dolomite filling, and (2) larger fractures with yellowish dolomiticrite or dolosparite fill and scattered angular chips of the dolomitized host rock (Fig. 8E). In the hairline fractures, dolomite crystal boundaries crosscut fracture walls, showing that dolomitization postdates fracturing. The blocky habit of the dolomite suggests that a possible precursor was low-magnesium calcite cement. In the wider fractures, brecciation was nearly *in situ* with little displacement of the clasts (Fig. 8F). The clasts are of similar composition and texture to the rock exposed at the fracture wall. Clast boundaries and fracture walls are sharp, with a few showing a thin rim of clear dolospar, which suggests that the late-stage fracturing postdates the main dolomitizing event. Sediment was injected into the veins, intimately permeating even the smallest veins; gravitational settling occurred with widening of the fractures. Some of these latter fractures may represent neptunian dikes.

The top of the dolomite, in Section 103-639A-8R, CC, is overlain by homogeneous pale yellow marlstone. The contact between these two lithologies was not recovered, but it is probably sharp. The marlstone is described in the following in more detail because of its importance in the geologic history of the underlying carbonate unit.

Unit III: Nannofossil Marlstone

The dolomite in Hole 639A is overlain by 48.9 m of pale yellow and pinkish gray, mottled marlstone, intercalated near the base with 10- to 20-cm-thick beds of a stiff marl, giving an apparent bedding inclination of 30°. Near the top of the unit, in Cores 103-639A-4R through 103-639A-6R, are some sandstone laminae and beds up to 10 cm thick that have been highly disturbed by drilling and, thus, have no identifiable sedimentary structures preserved. Marlstone is bioturbated and fractured, with hairline fractures dipping about 60° and stained yellow by limonite. Nannofossils and clay are the dominant components of the marlstone, with quartz and feldspar silt grains, mica, and glauconite in trace amounts. The biogenic component, except for the nannofossils, includes *Nanoconus*, calpionellids (Cores 103-639A-5R to 103-639A-8R), and trace amounts of foraminifers, mollusk debris, and radiolarians. Dolomite rhombs occur in traces near the base of the unit.

The foraminifers, calpionellids, and nannofossils indicate a Valanginian age, with the base of this unit of middle early Valanginian age (Moullade et al., this volume; Shipboard Scientific Party, 1987b). The unit is a hemipelagic deposit laid down at the outer, deeper continental shelf or upper slope environment. The sandstone intercalations near the top of the unit are probably turbidity current deposits.

The biostratigraphic age dating of Subunit VA in Hole 639D is based on calpionellids (Core 103-693D-5R), of which the presence of *Calpionella alpina*, *Crassicollaria massutiniana*, and *Crassicollaria brevis* indicates a middle late Tithonian age (*Crassicollaria* A Zone) (Shipboard Scientific Party, 1987b). The deeper cores (103-693D-6R to 103-693D-13R) are characterized by the presence of *A. lusitanica*, indicating a Tithonian age for Subunits VB and VC. This foraminifer, according to Hottinger (1967), was found in Morocco in Tithonian and Kimmeridgian age sediments; however, in the Bonniton H-32 well on the Grand Banks (fig. 24 in Jansa et al., 1980; Grant et al., this volume)—juxtaposed to Galicia Bank—*A. lusitanica* was not found in sediments older than Tithonian. Thus, a Tithonian age for the sediments enclosing *A. lusitanica* at Site 639 is most likely.

The dolomites in Holes 639D, 639B, and 639A generally lack identifiable fossils for biostratigraphic dating, but they overlie limestones dated as Tithonian. Daniel and Haggerty (this volume) identify benthic foraminifers revealed by fluorescence petrography in Sample 103-639A-10R-2, 16–21 cm, as a *Dorothia* sp. assigned to *D. cornula* (Reuss) and a trochamminid. These are neritic or upper bathyal forms that may be as young as Valanginian. On the basis of stratigraphic superposition and this biostratigraphic data, the dolomites may range in age from the late Tithonian to Valanginian, even though interpretation of dolomitization events at Site 639 indicates that a Valanginian age for the top of carbonate platform is very unlikely. In view of the age of the nearby Mesozoic carbonate platforms, we consider the dolomites to be late Tithonian to ?early Berriasian in age, in accordance with the age of the carbonate platforms in the Arosa Basin and the eastern Grand Banks (Grant et al., this volume).

DEPOSITIONAL ENVIRONMENT

Our interpretation of the depositional environment of the carbonates encountered at Site 639 is graphically summarized on Figure 9. The prominent bimodality of the dominant oncolith-skeletal-peloid wackestone to packstone microfacies of Subunit VC indicates sediment mixing from two sources. The finer fraction, dominated by hard, fine-sand-size peloids, is a facies commonly found in the shelf lagoon environment, such as on the western side of Andros Island, Bahamas. The biota associated with this microfacies is shallow marine and of normal salinity. However, the variety of the fauna in Subunit VC is less than that in the overlying Subunit VB; in particular, small benthic foraminifers are rare and dasycladacean algae are common. Such an assemblage is found in a shallow, slightly restricted marine environment. The fauna enclosed as oncolith nuclei are large foraminifers, algae, and/or mollusk debris; the oncoliths formed in a shallow subtidal to deep intertidal environment (Flügel, 1982). The strong micritization of the oncoliths is environmentally significant; it could be the result of intensive algal or fungal borings, but it also could be from the transformation of carbonates exposed to meteoric water. Thus, a shallower depositional environment is most likely for the oncolithic lithofacies at Site 639.

The skeletal-peloid packstone to wackestone lithofacies of Subunit VB has a richer faunal association, particularly of foraminifers, than that of Subunit VC. Large foraminifers, probably reworked from a shallower environment, are found as laminae in beds of intercalated marlstones. This may indicate that Subunit VB was deposited in a less restricted, more seaward marine environment than Subunit VC. Such an interpretation seems to be contradicted by the occurrence of reddish colored terrigenous sandstones and marls, which would favor deposition in a highly oxidized ?nearshore marine environment. The presence of fossil remains, including large foraminifers, and coated quartz

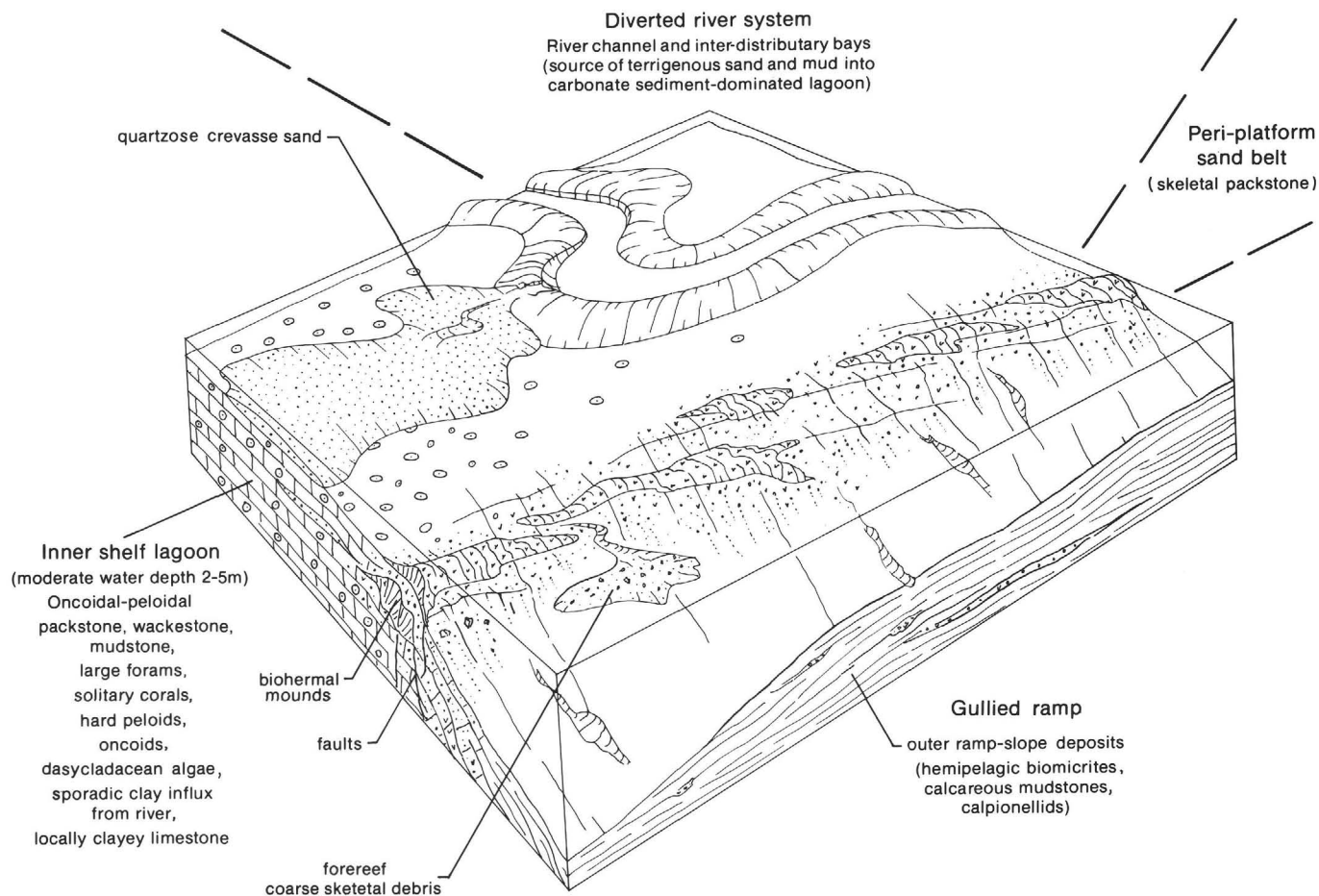


Figure 9. Block diagram portraying the depositional environmental setting of carbonates at Site 639.

grains in the sandstone indicates transport of clastics into the carbonate environment. The poor sorting and mostly angular shape of the clastic grains is indicative of a short transport distance.

Local tectonism probably increased the gradient of some of the streams, which would have resulted in clastics being transported farther onto the shelf into the carbonate depositional domain. An alternative explanation that the occurrence of clastics is the response of sea-level lowering is not supported by the enclosed fauna.

The importance of the clastics in providing relief for initiation of the Subunit VA bioherms cannot be established because of the limited core recovery, but a significant role appears probable. Furthermore, insufficient core recovery does not allow us to determine whether the biohermal limestones are *in-situ* low-relief mounds, a back-reef deposit, or debris from the lower flank of a larger reef structure. The presence of geopetal cavities, microbial crusts, sponges, and intercalations of quartz silty peloid packstones and wackestones with calpionellids and marly beds favors the interpretation of low-relief biohermal mounds, several tens of centimeters to several meters in height, in a moderate water depth (30–50 m) near the paleoshelf edge. Similar mounds, 1 to 2 m in height, are known from exposed Upper Jurassic limestones of the Lusitanian Basin and Algarve, studied by the senior author and described in part by Ellis (1984). We have indicated previously that the dolomites in Hole 639B were originally biohermal limestones; thus, we interpret these deposits to be part of the same stratigraphic horizon as the biohermal carbonates in Hole 639D.

That the echinoid-oolitic grainstone and packstone of Subunit IVA (Hole 639A) was deposited in a higher energy, shallower water environment than the limestones of Subunit IVB can be interpreted either as an indication of progressive shallowing of the carbonate platform surface or as the result of shelf edge morphology, because carbonate platforms commonly develop at the shelf edge (Jansa, 1981). No indication of a hard-ground was observed on the uppermost recovered dolomite core, which indicates that the top of the dolomite represents an erosional surface or that the contact was not recovered.

LIMESTONE DIAGENETIC HISTORY

The diagenesis of the limestones is relatively simple whereas that of the dolomites is exceptionally complex (Figs. 10 and 11) (Daniel and Haggerty, this volume). The hard peloids and oncoliths in the wackestone and packstones do not show any pronounced grain-surface deformation by the overburden, which indicates an early cementation. Similarly, geopetally filled cavities require early cementation for their preservation. Extensive development of syntaxial overgrowths on echinoid plates further confirms early diagenetic cement precipitation. The soft peloids are merged but not flattened, indicating that cementation occurred soon after deposition of some of the overburden. Evidence of fibrous, fringing, early submarine, or phreatic cements is conspicuously lacking. Calcite cement occurs rarely and is a blocky, low-iron variety, typical of burial-type cement. Molds from dissolved bioclasts are occluded by blocky sparry calcite, which is dominantly low ferroan, with some ferroan occurrences. One coral near the bioherm surface was replaced

with silica. The source of the silica could have been the sponges. Micrite "matrix" is extensive in these limestones and is associated with the occurrence of silt-size peloids. Considering that only minor compaction is observed, this part of the micrite represents an early diagenetic cement that probably precipitated at shallow depth (centimeters) beneath the sediment surface.

Stylolitization resulting in chemical compaction is very intensive in the limestones, leading in places to the removal of significant parts of the limestone, as evidenced the different lithofacies occurring on opposite sides of stylolitic seams. Stylolites were also avenues for migration of solutions, as suggested by the oxidation and partial dolomitization of sediments along some of the stylolites. Minor dedolomitization in Subunit VC has been related by Loreau and Cros (this volume) to a pre-late burial diagenetic event, resulting from freshwater alteration.

Early Diagenetic Structures in the Dolomitic Sequence

The final stages of the development of the carbonate platform are represented by carbonate strata that were post-depositionally dolomitized. Some textural features were preserved, thereby providing an insight into the environment of deposition of this unit. Cavity patterns and their infilling provide additional clues about sedimentary and diagenetic processes. The diagenetic pathways of the dolomite at Site 639 are diagrammatically summarized in Figure 10.

Sheetlike and irregularly shaped cavities are interpreted to be early diagenetic features resulting from the desiccation, shrinkage, and fracturing of unconsolidated carbonate sediment that experienced repeated subaerial exposure. Leaching of the exposed carbonate may have widened the early formed cavity system. These structures similar to "fenestrae" (Tebbutt et al., 1965; reviewed in Flügel, 1982) are found in frequently exposed intertidal flat sequences, where the exposure and weathering of sediments take place.

Birdseyelike structures preserved in the dolomites of Site 639A are nearly rounded, bubblelike cavities that were first described in shallow-water carbonate sequences, in association with decaying algal mats (Ham, 1952; Tebbutt et al., 1965). However, these structures are recognized as common to both carbonate and siliciclastic tidal sediments (Deelman, 1972; M. Sarti, unpubl. data, 1987). Birdseyes are gas bubbles that form within the sediment as a result of biotic or abiotic processes (see review in Flügel, 1982). Air bubbles developing in clastic, uncohesive, and organic-matter-free sediments are probably the result of air trapping during subaerial exposure and flooding in tidal zones (Deelman, 1972).

These data indicate that the carbonate precursor to the dolomite at Site 639 underwent subaerial exposure (shrinkage, leaching of carbonates, and perhaps even evaporites precipitation). Gas-bubble porosity identified near the top of carbonate se-

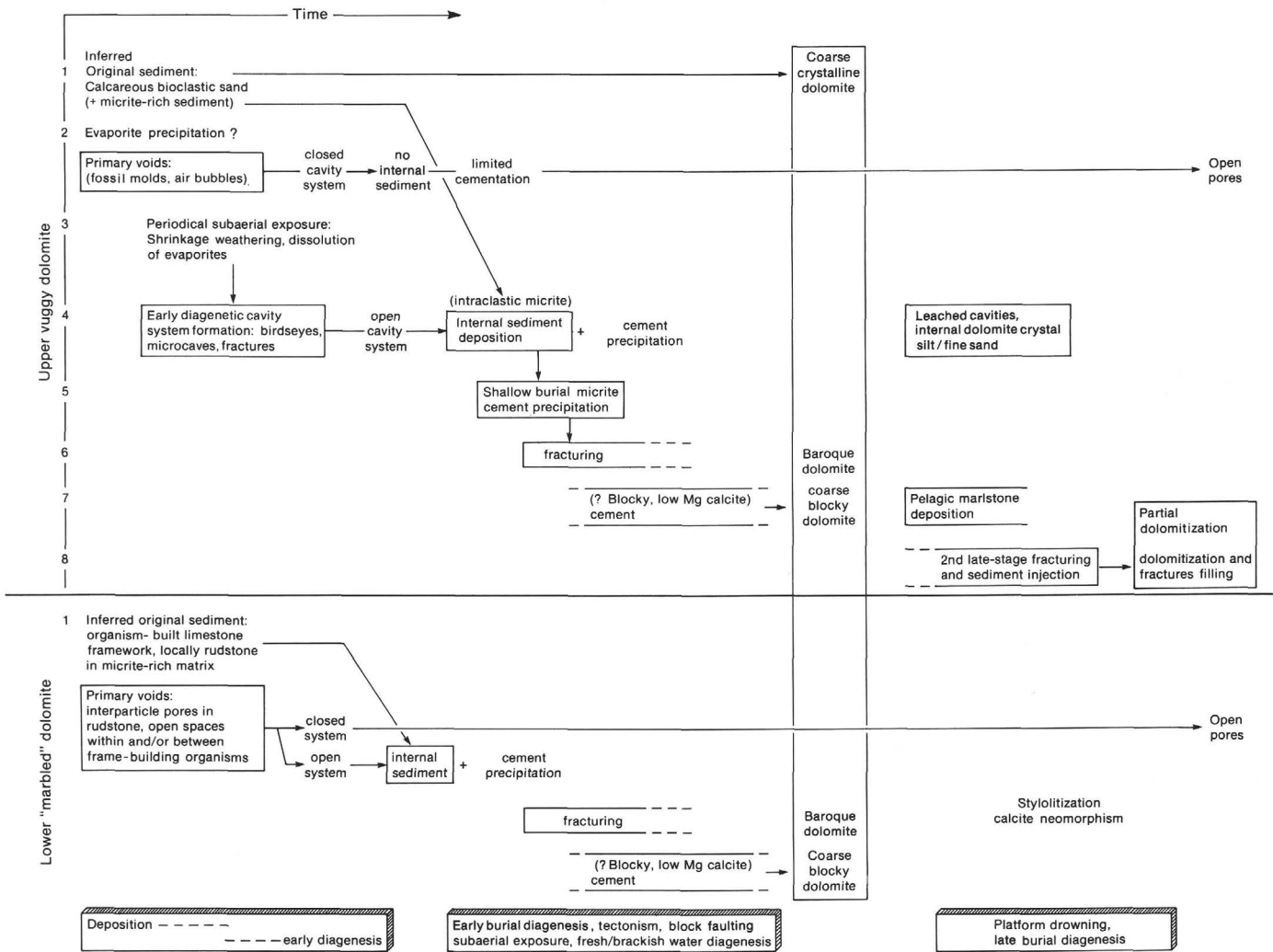


Figure 10. Diagram showing the major diagenetic pathways of dolomites at Site 639. A correlation with the structural evolution of the carbonate platform is shown at the base of the diagram. For discussion, see text.

GSC

quence is a good indicator of deposition in an intertidal environment. The presence of vadose crystal silt in some of the cavities suggests that the sediment periodically resided above the water table. The baroque dolomite observed in Sample 103-639A-10R-2, 16–24 cm, may be a pseudomorph after evaporite minerals (Friedman, 1980), which would suggest temporary hypersaline conditions (see also Haggerty and Smith, this volume).

However, baroque-type dolomite also occurs as cavity-filling cement and fracture lining (Fig. 8E), and in this case it is not an obvious replacement of evaporite minerals. Folk and Assereto (1974) typically refer this type of dolomite to dolomitization in the mixing zone of ground and saline waters. Its isotopically light $\delta^{18}\text{O}$ signature (Haggerty and Smith, this volume) indicates that this dolomite could form from hypersaline brines associated with an evaporative loop during shallow burial or by re-equilibration during deep burial, although Loreau and Cros (this volume) use the same values to argue for a freshwater influence.

Broken, euhedral crystals of clear dolomite and crystal silt are common components of the internal sediment fill of fractures and microcaves at Hole 639A (Fig. 8F). These broken crystals represent reworked fragments of dolomite crystals from a poorly lithified sucrosic dolomite at the top of the platform. They are interlayered with laminae of clayey dolomicrite. Some of the voids are filled with yellowish clay and silt. The isotopic composition of the yellow silt, with $\delta^{13}\text{C}$ ranging from +2 to +3 and $\delta^{18}\text{O}$ from -4 to +3 (Loreau and Cros, this volume), is indicative of early diagenetic dolomite replacing marine carbonate. This dolomite represents the second(?) stage of dolomitization that occurred immediately after initial drowning of the carbonate platform.

Dolomitization

Interpretation of the petrographic, tectonic, geochemical, and isotopic data for the dolomites of Site 639 results in contradictory interpretations of the dolomitizing event (compare with Loreau and Cros, this volume; Haggerty and Smith, this volume). The Valanginian marlstone separated by an unconformity from underlying carbonate shows minor signs of dolomitization. Isolated dolomite crystals were observed to have grown diagenetically into the sediment near the base of the formation, but no massive replacement has occurred. This late mild metasomatism was affected by contact with the dolomite and circulating formation water, postdating the main dolomitizing event (see "Site 639" Chapter; Shipboard Scientific Party, 1987b). The brittle fractures healed by calcite and then dolomitized together with the host rock indicate that early fracturing and rock lithification predate dolomitization and consequently, predate deposition of the Valanginian marls. Dolomitization is postfracturing, which suggests that it occurred on an already fault-dissected margin. Less intensive dolomitization in Hole 639D is best explained by the different elevation of the site in respect to the dolomitization front. The downward-extending dolomitization front and the distribution of the dolomite across stratigraphic boundaries imply that one viable mechanism of dolomite formation could be the mixing of dolomitization fluids (Badiozamani, 1973; Folk and Land, 1975). If this is the case, the dolomitization of carbonates at Site 639 must have happened early, soon after the establishment of a regional fluid-mixing stage, and would have been completed before the drowning of the platform. The geochemical data (Haggerty and Smith, this volume) do not support freshwater mixing. Trace amounts of sulfate mineral inclusions in the dolomite suggest that dolomitization occurred by

concentrated seawater in the form of oxidizing hypersaline brines originating in an evaporitic environment.

The positive carbon isotopic composition of dolomite ($\delta^{13}\text{C}$ averages +1.5) is consistent with marine sources (Haggerty and Smith, this volume), but according to Loreau and Cros (this volume), similar values are also found in dolomites originating by freshwater/salt-water mixing. The very light oxygen isotopic composition, which exhibits a range of values from -8 to -11.3 for $\delta^{18}\text{O}$, may point to a late diagenetic, low-temperature "metasomatic" origin of dolomitization (Mattes and Mountjoy, 1980). Fluid-inclusion homogenization temperatures ranging from 67° to 84°C (Haggerty and Smith, this volume) support such an interpretation. The latter authors interpret the oxygen isotope data and homogenization temperatures to be the result of shallow-burial dolomitization by oxidizing, hypersaline brines associated with a higher geothermal gradient. Alternatively, they could be a consequence of a diagenetic overprint during deeper burial with concurrent re-equilibration of the oxygen isotopic composition of the dolomite, as well as the homogenization temperatures of the fluid inclusions (Haggerty and Smith, this volume). The homogenization temperatures, without pressure correction and assuming the inclusions have not stretched during deeper burial, can be used as a very crude dipstick to test the conditions at which the dolomite crystals were formed. If we consider the temperature of the evaporitic environment at the top of carbonate platform to have been 35°C (McKenzie et al., 1980), then a rise of 20°–30°C would have resulted from burial. Assuming a geothermal gradient of 35°C/1000 m, it can be argued that the main dolomitization event may have occurred in a limestone sequence upon burial by approximately 500 m of sediments. The subsequent occurrence of several minor episodes of dolomitization is associated with fracture filling and the filling of secondary, leached voids.

Late Fracturing

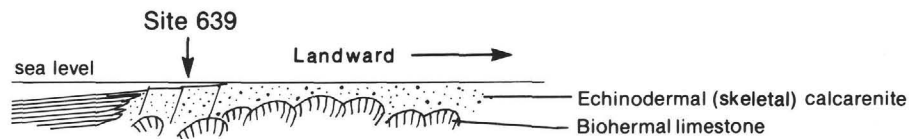
Although the yellowish sediment that fills the late-stage fractures is itself dolomitic and dolospar rims are developed around some of the clasts filling fractures (Fig. 8F), we concluded that no major whole-rock recrystallization took place after the latest set of fractures was formed. Mild replacement occurred as a result of contact with the dolomitic host rock, in a similar fashion to what is envisaged for the overlying pelagic drape. Some of the yellowish sediment is gravitationally settled within the cracks, but other occurrences seem to be injected as a result of fracturing, implying that the late-stage fracturing postdates both the major dolomitization event and the deposition of post-carbonate-platform sediments.

This evidence from the rock record demonstrates that a long-lasting episode of brittle fracturing is sandwiched between post-lithification and immediate predolomitization and post-early Valanginian platform drowning, encompassing a period of about 4 m.y. Different types of fracture filling formed depending upon the diagenetic environment in which the fracturing occurred. Sediment-free brittle fractures formed early, when the pelagic cap was absent. These fractures are most probably Tithonian in age. Sediment-injected fractures formed later, after the pelagic sediment had been deposited, and we conclude that this formation was probably during the Valanginian.

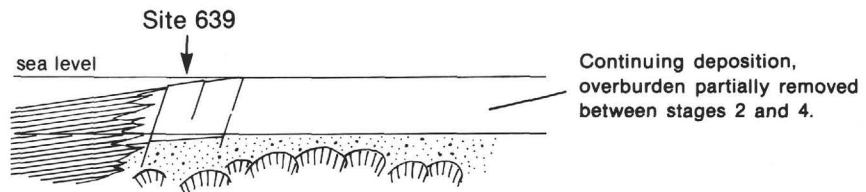
We relate fracturing to tectonic processes at the margin. The first period of faulting (Fig. 11) resulted in downfaulting of the carbonate platform edge, as indicated by the varying lithofacies in the studied holes of Leg 103. The second period of faulting is poorly constrained, but it is indicated by exposure and possible erosion of the carbonate platform during Berriasian time. Faulting and fracturing of the carbonate platform is seen as providing conduits through which hypersaline brines migrated and do-

STAGE 1: TITHONIAN

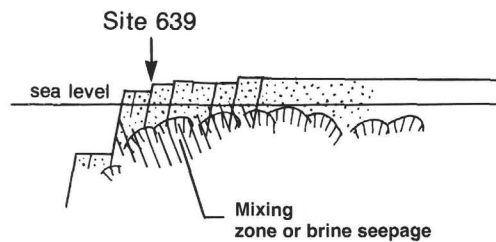
Shallow-water deposition; sandy and muddy facies, subaerial and vadose diagenesis, and local evaporite nodules

**STAGE 2: BERRIASIAN**

Continued subsidence and shallow-water deposition, shallow burial cementation, neomorphism, pre-dolomitization fracturing and cementation, and minor faulting

**STAGE 3: SHALLOW BURIAL DOLOMITIZATION**

Platform breakup, faulting, subaerial exposure of carbonate at uptilted edge, fluids mixing or brines replacing and dolomitizing, erosion, ? karst topography; dolomite silt infilling cavities.

**STAGE 4: EARLY VALANGINIAN**

Platform collapse and drowning, backfaulting and tilting, subsidence, post-dolomitization fracturing and sediment injection, and minor dolomitization of pelagic drape.

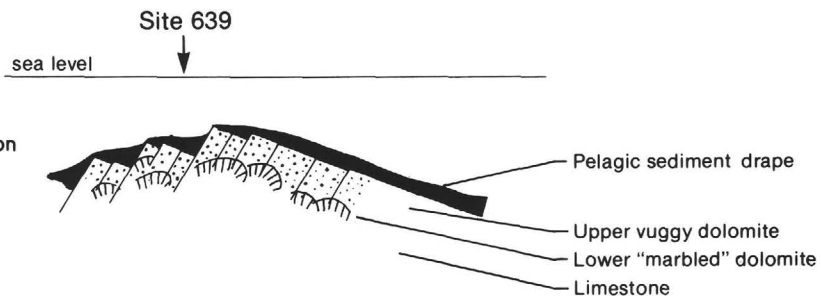


Figure 11. Basic steps of the structural evolution of the carbonate platform at Site 639, as inferred from the diagenetic history of the dolomites. For discussion, see text.

lomitized the limestone (see discussion by Haggerty and Smith, this volume). The third set of fractures, recognized by sediment injection in the previous fractures, indicates that movement along faults persisted long after the drowning and burial of the carbonate platform marginal blocks. Alternatively, some of these later faults could be the result of another major tectonic period during which the whole tectonic blocks were downfaulted and rotated eastward in the ?late Valanginian.

GEOLOGIC HISTORY OF THE CARBONATE PLATFORM

The geologic history of the carbonate platform is reconstructed from the data presented in the preceding and from auxiliary evidence from synchronous carbonate platforms formed during the Late Jurassic on the northern central North Atlantic margins.

We have indicated that the carbonates encountered at Site 639 (Fig. 13) represent a carbonate platform. This interpretation is supported by the thickening of the carbonates in an offshore direction to Hole 639A (Fig. 2). Less conclusive evidence is that some of the carbonates in Hole 639D may represent slope debris and that the top of the platform was a shoal. According to interpretation of the seismic data (Fig. 2), the carbonates unconformably overlie clastic rocks. The maximum thickness of the carbonate platform could be 420 m, based on a compressional velocity of 4.5 km/s. Because clastic beds are intercalated with the carbonates, the thickness of the platform is accordingly less. According to our estimates (Fig. 3) 287 m of the carbonate sequence was penetrated at Site 639. The carbonates are of Tithonian to ?early Berriasian age. From the seismic data, it is not improbable that the carbonates may extend down into Kimmeridgian.

The depositional setting for the carbonates was a shelf lagoon (Fig. 9) comparable to the western side of Andros Island, Bahamas, or an inner shelf environment similar to that of northeast Australia. Clastics intercalated within the limestone sequence, poor sorting and angular grain shape, and a high concentration of feldspars point to a low-relief, continental, acidic-type (granodiorite-dominated) basement, subaerially exposed not far from the depositional site. Thus, the carbonate platform at the western side of Galicia Bank could have been a localized rimmed platform, developed around a low-relief island formed atop the basement block.

The recovered cores do not provide sufficient information about more subtle environmental changes in the platform development. The facies indicate progressive deepening as result of Tithonian transgression in Hole 639D, which reversed during the late Tithonian to a shallowing trend, in turn leading to the development of shallow, high-energy "skeletal-oolitic shoals" that buried the bioherms (Hole 639A). This change correlates with the eustatic sea-level lowering that occurred just prior to deposition of the *Crassicolaria* A Zone, according to Haq et al. (1987). Further support for eustatically controlled environmental change can be found in the history of Late Jurassic carbonate platforms at the circum-North Atlantic margins.

During the Late Jurassic, the development of carbonate platforms along the North Atlantic margins become extensive (Jansa, 1981; Jansa and Wiedmann, 1982). Because such development was synchronous on the separated continental plates (African, North American, and European), climate and eustatics were probably the principal controlling factors in the evolution of the platforms. The most proximal carbonate platform eastward of Galicia Bank is on the eastern flank of the Arosa Basin. The sequence is about 400 m thick and is dominated by shallow-water carbonates. The similar thicknesses of these two platforms, even with the Galicia Bank platform located 200 km west of the Arosa Basin, supports our interpretation that the carbonate mass at Site 639 is part of a platform and not a ramp, as suggested by Moullade et al. (this volume). To the north, at Deep Sea Drilling Project Site 401 on the Meriadzek Terrace in the Bay of Biscay, 94 m of Upper Jurassic to Lower Cretaceous pellet-intraclast grainstone and packstone, containing some debris of corals, hydrozoans, and rare calpionellids, was recovered (Monadert, Roberts, et al., 1979); this lithology is similar to that encountered at Site 639. Limestones at this locality are unconformably overlain by upper Aptian chalk. The third area of concern is the Carson Sub-basin on Grand Banks (Jansa and Wade, 1975; Jansa et al., 1980; Grant et al., this volume) where Kimmeridgian-Tithonian neritic limestones and shales were penetrated during oil exploration. The Tithonian section encountered in the Bonniton well is 200 m thick and consists of shallow-water limestone overlying medium gray, calcareous shale at a sharp basal contact (see Fig. 13 in Grant et al., this volume). Upward in the section, the limestone becomes intercalated with marls containing large foraminifers (*A. lusitanica*) and calpionellids. Another bed of skeletal packstone with coral debris and minor oolitic grains and oncoliths occurs at the top of the Tithonian. This upper limestone is overlain at a sharp contact by brownish gray calcareous shale, with minor silty mudstone beds. The shale, which contains scattered calpionellids, is of Berriasian-Valanginian age (Jansa et al., 1980). Even though there is a sharp lithologic boundary at the top of the limestone, indicating perhaps a sharp environmental change and possibly a diastem, paleontology suggests continuous deposition. However, paleontological evidence for the presence of Berriasian at this locality is weak.

Several conclusions can be derived from the regional distribution of carbonate platforms of the Late Jurassic. The Titho-

nian carbonate platform of the Galicia Bank is located between the platforms of the Arosa Basin and of the Carson Sub-basin. This suggests that the Galicia carbonate platform was probably part of a broader carbonate shelf that evolved during the Tithonian (Fig. 12). The intercalations of limestones and shales in the Upper Jurassic of the Carson Sub-basin are similar to those in Hole 639D (Subunit VC), denoting *in-situ* carbonate deposition for the hole. Furthermore, the similarity in lithologic composition of the Tithonian limestones between Galicia Bank, Carson Sub-basin, and Meriadzek Terrace suggests that the sea covering the carbonate shelf was very shallow.

A disruption in deposition occurred in all three areas very early in the Cretaceous, with the shortest disruption on the Grand Banks and longest one at the Meriadzek Terrace. Only on Galicia Bank has intensive dolomitization been observed. What makes the western margin of the Galicia Bank different from other carbonate platforms is the extensive fault tectonics, development of a postdepositional unconformity, and, with less certain identity, subaerial exposure and erosion. Geochemical and isotopic data clearly indicate the importance of postdepositional fluids on dolomitization at Site 639. The observed $\delta^{18}\text{O}$ -depletion shift from meteoric water and petrographic data (Fig. 13) discussed previously point to the dolomitization as being late diagenetic and low-temperature and that it occurred soon after tectonic faulting began, when the platform was still buried under several hundred of meters of sediment. The fluid pathways allowed oxidizing, sulfate-bearing, evaporitic brines to displace less saline and less dense pore fluids during shallow burial of the platform in a higher geothermal-gradient regime associated with rifting, which aided the dolomitization process. The source of the evaporitic brines was the localized evaporitic environment, which developed as the result of a combination of tectonics (faulting) and eustatic sea-level lowering. An undetermined thickness of sediments was removed at the unconformity during subaerial exposure prior to the platform drowning. This erosion could have been accentuated by a major eustatic sea-level drop that occurred during the early Valanginian (126 Ma; Haq et al., 1987). After that the platform was drowned, dated paleontologically as prior to deposition of Calpionellid Zone E, the middle part of the lower Valanginian (Moullade et al., this volume). It remains unclear as to whether this initial carbonate platform drowning is the result of eustatic sea-level rise or from a renewed period of tectonism as the rifting of the outer Galicia margin progressed.

One of the main results of our diagenetic and dolomitization studies is that they provide a time constraint on the dating the major tensional period on western margin of the Galicia Bank. The difference in intensity of dolomitization between Holes 639A and 639D indicates that only minor faulting occurred prior to the main post-late Tithonian dolomitization. The major tectonic episodes are concurrent and in part postdolomitization. The first tectonic episode, which is represented by block faulting, subaerial exposure, and partial erosion of the carbonate platform, is not younger than early Valanginian and not older than late Tithonian. Considering that an undetermined thickness of sediments was deposited on the top of the carbonate platform and later removed at the erosional unconformity, the time of tectonism can be further bracketed to ?late Berriasian-earliest Valanginian. The second period of tectonism is poorly established by drilling results, but can be better identified by seismic data (Fig. 1). The tectonism that resulted in downfaulting and rotation of the tectonic blocks to the east occurred after deposition of seismic Unit 5, which was interpreted by the Shipboard Scientific Party (1987b) as corresponding to upper Valanginian turbidites, and prior to or during deposition of untested seismic Subunit 4 (Fig. 1 and the wedge-shaped unit

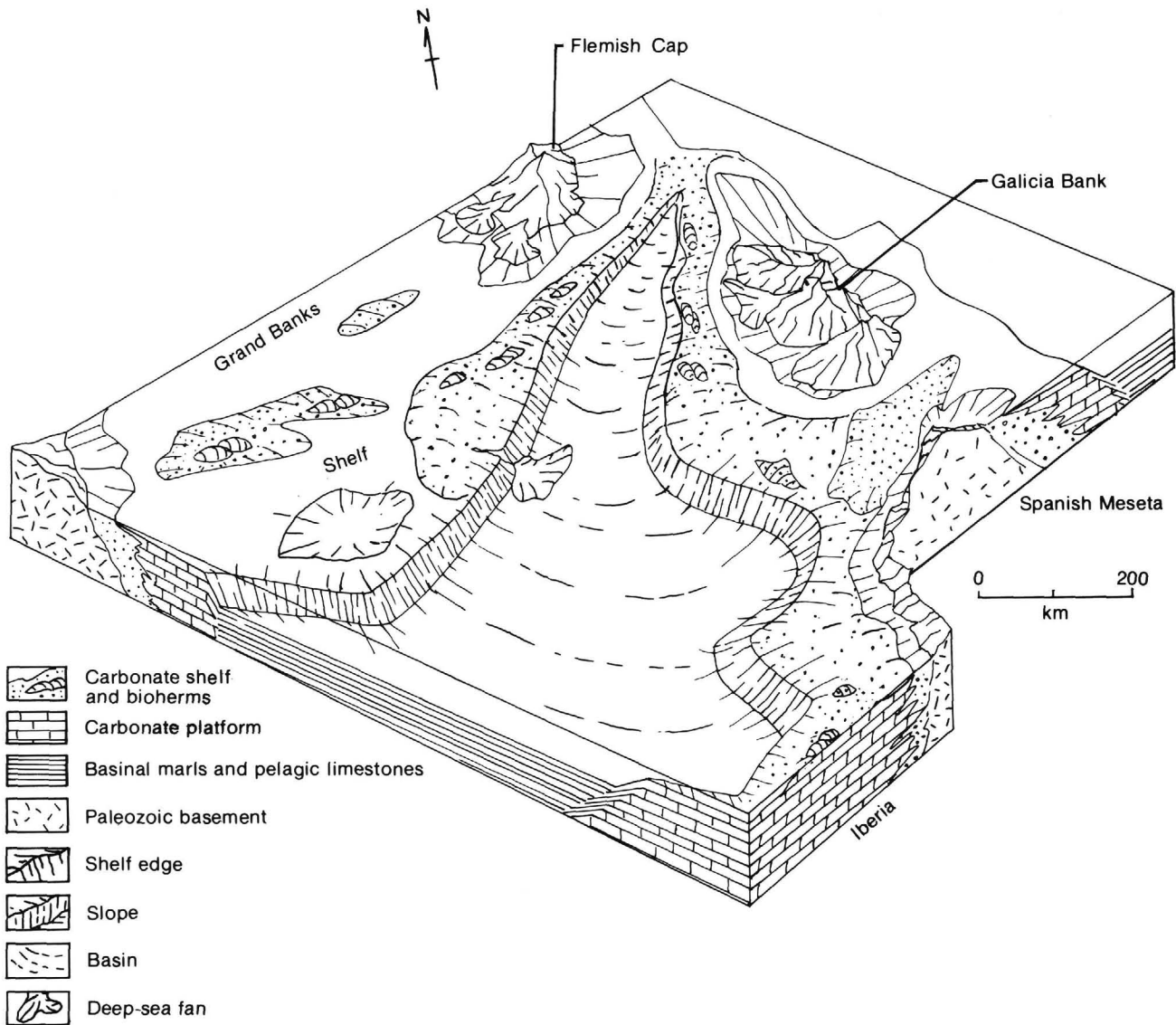


Figure 12. Paleogeographic reconstruction of the Iberia-Grand Banks region during the Tithonian.

underlying reflector V on Fig. 2). The age of this unit from the seismic and drilling data is reasonably constrained as Hauterivian.

Miocene sediments overlie the downfaulted limestone blocks, except at Hole 639C, where the dolomites are overlain by reddish brown unfossiliferous clay. A similar clay is widespread in the central North Atlantic, where it was described as Plantagenet (Jansa et al., 1979) of late Cenomanian to Eocene age. Such shale is deposited in deep water, below the carbonate compensation depth. The occurrence of such a shale at Hole 639C indicates that the downfaulted edges of the carbonate platform subsided to abyssal depth during the Late Cretaceous to early Tertiary.

ACKNOWLEDGMENTS

The authors express their gratitude to A. Edwards for assistance in seismic data interpretation and to two unknown reviewers for helpful critical comments that improved the manuscript. We are indebted to the ODP shipboard staff for their assistance during Leg 103 and to G. Boillot and E. L. Winterer for encouragement and advice through the cruise. Financial support for M. C. Comas was provided by the Spanish Committee for the ODP and Consejo Superior de Investigaciones Cientificas. M. Sarti was financially supported by the Consiglio Nazionale delle

Ricerca (Grants No. 86.00995.05 and 87.00707.05). L. Jansa acknowledges the support of the Geological Survey of Canada in this study and is thankful to G. Grant for drafting and N. Koziel for typing of the manuscript. J. Haggerty thanks JOI-USSAC for the financial support of her research. This is Geological Survey of Canada Contribution no. 2004.

REFERENCES

- Badiozamani, K., 1973. The Dorag dolomitization model; application to the Middle Ordovician of Wisconsin. *J. Sediment. Petrol.*, 43: 965-984.
- Boillot, G., Winterer, E. L., et al., 1987. *Proc. ODP, Init. Repts.*, 103: College Station, TX (Ocean Drilling Program).
- Deelman, J. C., 1972. On mechanism causing birdseye structures. *Neues Jahrb. Geol. Palaeontol. Abh.*, 12:582-595.
- Dupeuble, P.-A., Boillot, G. and Mougenot, D., 1987. Upper Jurassic-lowest Cretaceous limestones dredged from the western Galicia margin. In Boillot, G., Winterer, E. L., et al., *Proc. ODP, Init. Repts.*, 103: College Station, TX (Ocean Drilling Program), 99-106.
- Ellis, P. M., 1984. Upper Jurassic carbonates from the Lusitanian Basin, Portugal, and their subsurface counterparts on the Nova Scotia Shelf [Ph.D. thesis]. Open Univ., Milton Keynes, U.K.
- Flügel, E., 1982. *Microfacies Analysis of Limestone*: Berlin (Springer-Verlag).

- Folk, R. L., and Assereto, R., 1974. Giant aragonite rays and baroque white dolomite in tepee fillings, Triassic of Lombardy, Italy. *Annu. Meet. Program Soc. Econ. Paleont. Mineral.*, 34-35.
- Folk, R. L., and Land, L. S., 1975. Mg/Ca ratio and salinity: two controls over crystallization of dolomite. *AAPG Bull.*, 59:60-68.
- Friedman, G. M., 1980. Dolomite is an evaporite mineral: evidence from the rock recorded and from sea-marginal ponds of the Red Sea. In Zenger, D. J., Dunham, J. B., and Ethington, R. L. (Eds.), *Concepts and Models of Dolomitization*: Spec. Publ. Soc. Econ. Paleontol. Mineral., 28:200-203.
- Ham, W. E., 1952. Algal origin of the "birdseye" limestone in the Mc-Lish Formation. *Proc. Okla. Acad. Sci.*, 33:200-203.
- Haq, B. J., Hardenbol, J., and Vail, P. R., 1987. Chronology of fluctuating sea levels since the Triassic. *Science*, 235:1156-1167.
- Hottinger, L., 1967. Foraminifères imperforés du Mésozoïque Marocain. *Notes Mem. Serv. Geol. Morocco*, 209.
- Jansa, L. F., 1981. Mesozoic carbonate platforms and banks of the eastern North American margin. *Mar. Geol.*, 44:97-177.
- Jansa, L. F., Enos, P., Tucholke, B. E., Gradstein, F. M., and Sheridan, R. E., 1979. Mesozoic-Cenozoic sedimentary formations of the North American Basin; western North Atlantic. In Talwani, M., Hay, W., and Ryan, W.B.F. (Eds.), *Deep Drilling Results in the Atlantic Ocean: Continental Margins and Paleoenvironment*: Am. Geophys. Union, Maurice Ewing Ser., 3:1-57.
- Jansa, L. F., Remane, J., and Ascoli, P., 1980. Calpionellid and foraminiferal-ostracod biostratigraphy at the Jurassic-Cretaceous boundary offshore eastern Canada. *Riv. Ital. Paleont.*, 86:67-126.
- Jansa, L. F., Steiger, T. H., and Bradshaw, M., 1984. Mesozoic carbonate deposition on the outer continental margin off Morocco. In Hinz, K., Winterer, E. L., et al., *Init. Repts. DSDP*, 79: Washington (U.S. Govt. Printing Office), 857-891.
- Jansa, L. F., and Wade, J. A., 1975. Geology of the continental margin off Nova Scotia and Newfoundland. In van der Linden, W.J.M., and Wade, J. A. (Eds.), *Offshore Geology of Eastern Canada, 2: Regional Geology*: Geol. Surv. Can., 74-30:51-106.
- Jansa, L. F., and Wiedmann, J., 1982. Mesozoic-Cenozoic development of the eastern North American and northwest African continental margins: a comparison. In von Rad, U., Hinz, K., Sarnthein, M., and Seibold, E. (Eds.), *Geology of the Northwest African Continental Margin*: Berlin (Springer-Verlag), 215-269.
- Mattes, B. W., and Mountjoy, E. W., 1980. Burial dolomitization of the Upper Devonian Miette Buildup, Jasper National Park, Alberta. In Zenger, D. H., Dunham, J. B., and Ethington, R. L. (Eds.), *Concepts and Models of Dolomitization*: Spec. Publ. Soc. Econ. Paleontol. Mineral., 28:259-297.
- McKenzie, J. A., Hsü, K. J., and Schneider, J. F., 1980. Movement of subsurface water under the sabkha, Adu Dhabi, U.A.E., and its relation to evaporite-dolomite genesis. In Zenger, D. J., Dunham, J. B., and Ethington, R. L. (Eds.), *Concepts and Models of Dolomitization*: Spec. Publ. Soc. Econ. Paleontol. Mineral., 28:11-30.
- Montadert, L., and Roberts, D. G., 1979. *Init. Repts. DSDP*, 48: Washington (U.S. Govt. Printing Office).
- Montadert, L., Winnock, E., Delteil, J. R., and Grau, G., 1974. Continental margin of Galicia-Portugal and Bay of Biscay. In Burk, A., and Drake, C. L. (Eds.), *Geology of Continental Margins*: Berlin (Springer-Verlag), 323-342.
- Mougenot, D., Capdevila, R., Palain, C., Dupeuble, P.-A., and Maufret, A., 1985. Nouvelles données sur les sédiments anté-rift et le socle de la marge continentale de Galicia. *C. R. Acad. Sci. Ser. 2*, 301: 323-328.
- Shipboard Scientific Party, 1987a. Introduction, objectives and principal results: Ocean Drilling Program Leg 103, west Galicia margin. In Boillot, G., Winterer, E. L., et al., *Proc. ODP, Init. Repts.*, 103: College Station, TX (Ocean Drilling Program), 3-17.
- , 1987b. Site 639. In Boillot, G., Winterer, E. L., et al., *Proc. ODP, Init. Repts.*, 103: College Station, TX (Ocean Drilling Program), 409-532.
- Tebbutt, G. E., Conley, C. D., and Boyd, D. W., 1965. Lithogenesis of a distinctive carbonate rock fabric. *Contrib. Geol.*, 4:1-13.

Date of initial receipt: 23 March 1987

Date of acceptance: 21 December 1987

Ms 103B-122

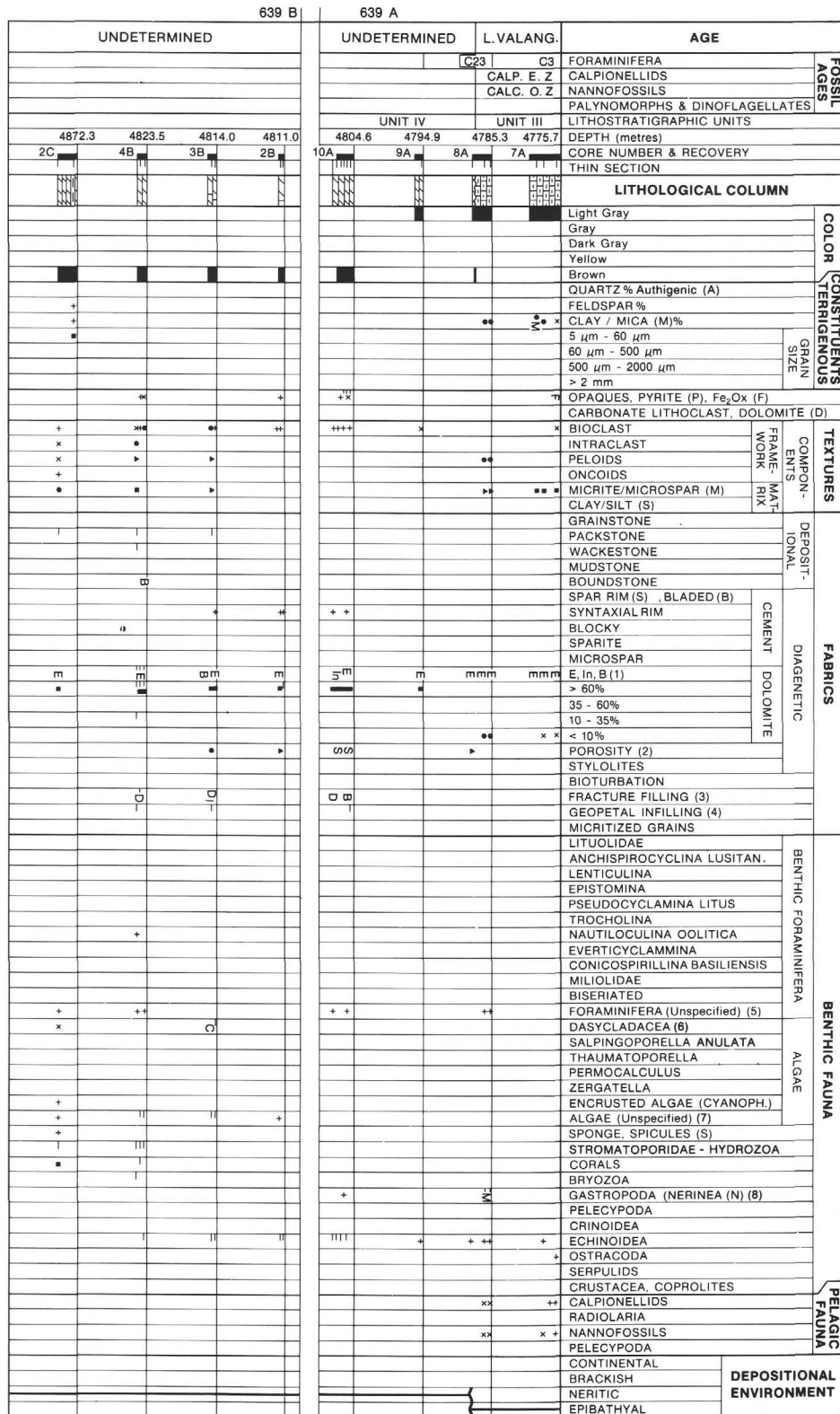
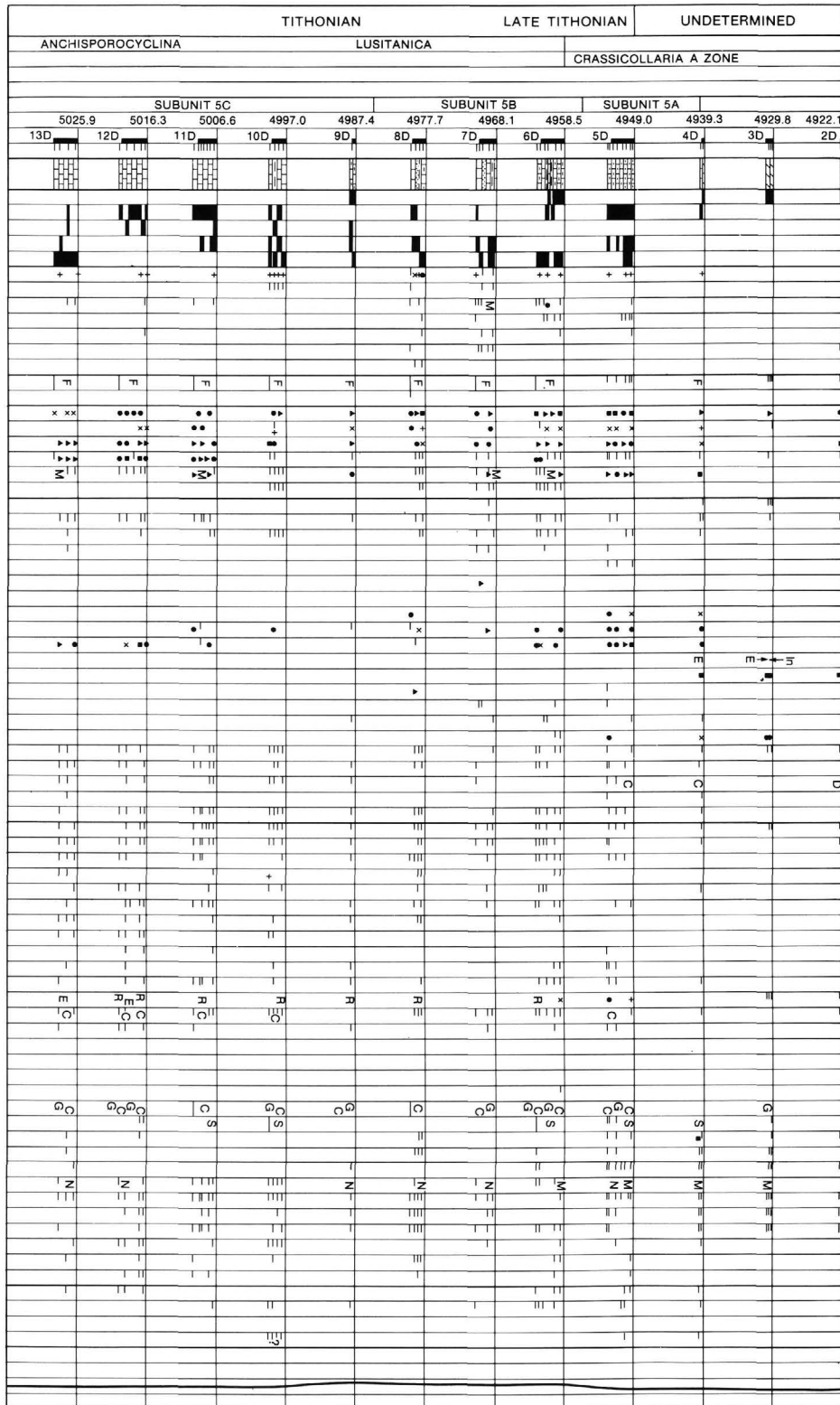


Figure 13. Geologic chart for the carbonate sequence at Site 639. Plot shows lithology, unit boundaries, ages, and composition (components and textural parameters) derived from thin section studies.



LEGEND

< 1% (or Trace) +
 1 - 5% x
 5 - 20% ●
 20 - 50% ▲
 50 - 100% ■
 PRESENT ■

(1) DOLOMITE:
 E Equant anhydrous
 In Inclusion rich
 B Blocky

(2) POROSITY:
 S Secondary

(3) FRACTURE FILLING:
 Bq Baroque

(4) GEOPETAL INFILLING:
 D Dolomite
 I Internal sediment
 C Calcite

(5) FORAMINIFERA:
 R Rectocyclammina
 E Encrusting foram.

(6) DASYCLADACEA:
 C Codiaceae

(7) ALGAE (Unspecified):
 G Gymnocodiaceae
 C Cyanophyceae
 S Solenoporaceae

(8) GASTROPODA:
 M Mollusca

Figure 13 (continued).